UNIVERSITY OF TRENTO

DOCTORAL THESIS

A Perturbational Approach to Understanding the Neural Basis of Resting-State Functional Connectivity

CAROLA CANELLA

Advisor: Alessandro Gozzi

A thesis submitted in fulfilment of the requirements

for the degree of Doctor of Philosophy in the:

Doctoral School in Cognitive and Brain Sciences, University of Trento

Center for Neuroscience and Cognitive Systems,

Istituto Italiano di Tecnologia

29 June 2020

Abstract and declaration

Declaration

This dissertation is the result of my own work unless specifically indicated in the text as the outcome of a collaboration, or cited and acknowledged as material from another source. It has not been previously submitted, in part or whole, to any university of institution for any degree, diploma, or other qualification.

Signed:_____

Date:_____

CAROLA CANELLA

University of Trento, Doctoral School in Cognitive and Brain Sciences
Istituto Italiano di Tecnologia, Center for Neuroscience and Cognitive Systems
Doctor of Philosophy

A perturbational approach to understanding the neural basis of Resting-State Functional Connectivity

CAROLA CANELLA

Abstract

Spatiotemporal correlations in the resting-state fMRI (rsfMRI) signal are commonly interpreted as an index of reciprocal interareal communication and functional connectivity. However, structurally based models of rsfMRI connectivity have not been comprehensively validated through experimental manipulations in the living brain.
Perturbational approaches are critically required for a deeper understanding of brain-wide rsfMRI coupling for two main reasons. First, the correlative nature of rsfMRI makes measures of functional connectivity fickle indicators of direct interareal interaction, as synchronous signals could reflect the contribution of global fluctuations, or could be driven by spatially remote functional interactions with a third region. Second, a deeper understanding of the fundamental elements and dynamic rules underlying the establishment of rsfMRI coupling is required to reliably back-translate clinical alterations in rsfMRI connectivity into testable neurophysiological events and models that can help understand, diagnose or treat brain disorders.

By allowing to link specific neural events to brain-wide patterns of brain activity, the combined use of rsfMRI and neuro-perturbational techniques offer the opportunity to bridge this knowledge gap, enabling a disambiguation of the correlative nature of rsfMRI coupling. Using this approach, here we show that chronic silencing of the prefrontal cortex (PFC) via overexpression of a potassium channel results in paradoxical rsfMRI overconnectivity of thalamo-cortical components of the mouse default mode network (DMN). Acute chemogenetics silencing of the PFC produced analogous patterns of rsfMRI oversynchronization, an effect that was functionally relayed to wider cortical areas by polymodal thalamic regions. Importantly, in vivo electrophysiological recordings showed that PFC silencing is associated with reduced gamma power and prominently increased slow oscillatory activity. The observed breakdown between cortical output and rsfMRI coupling challenges prevailing structurally based models of rsfMRI connectivity and suggests that long-

range functional coupling is critically orchestrated by locally and remotely generated slow-oscillatory rhythms.

Acknowledgements

When I arrived in Rovereto, some years ago, I was an aspiring researcher, with the dream of becoming a great scientist. Today, I'm not the scientist I wanted to be; but I am the person I want to be. And this was possible thanks to the people I met here in Rovereto.

To Alessandro Gozzi and the “crew”: Marco Pagani, Ludovico Coletta, Daniel Gutierrez, Federico Rocchi, Alberto Galbusera, Alexia Stuefer, Elizabeth de Guzman, Neah Singh, Ilena Alvino, Caterina Montani, Chiara Franceschi, David Sastre, Fabio Gatto, Lorenzo Grilli and also previous members: Adam Liska and Alessia de Felice.

To all my friends in IIT (Giulia, Rossella, Sara, Florian, Denise, Laura) thank you for your unconditional friendship, which I will always cherish.

To all the friends in Block3, Arianna, Caterina, Mavi, Alessio and the crazy Monday climbing and drinking beers.

To all the people who have always been: Rosanna and Nicolò, thanks to your support I’ve manage to be here. To zio Paolo, and his enthusiasm to start again.

To my crazy family, to Caterina, Chiara and Elena, to my friends from Caselle, to Gabriele and Giorgio (always ready to celebrate my goals).

To all the people, that render these years wonderful.

Contents

List of Figures

Nomenclature and Acronyms

Ach – Achetylcholine

AchR – Achetylcholine Receptor

Arch – Archearhodopsin

ASD – Autism Spectrum Disorder

BOLD – Blood-Oxygen-Level-Dependent

CAP – Co-Activation Pattern

Cg – Cigulate Cortex

ChR2 – channelrhodopsin 2

CNO – Clozapine-N-Oxide

CNTNAP2 – contactin associated protein-like 2

DMN – Default-Mode Network

DREADD – Designer Receptor Activated Exclusively by Designer Drug

E/I – Excitatory/Inhibitory

FC – Functional Connectivity

FDR – False-discovery Rate

fMRI – functional MRI

FEW – Family-wise error

GFP – Green Fluorescent Protein

Gu – Gustatory Cortex

hM4Di – modified form of the human M4 muscarinic (hM4) receptor.

hM3Dq - modified form of the human M3 muscarinic (hM3) receptor.

hSyn – human Synapsin

Ins – Insula

KORD – K-opiod receptor DREADD

LCN – Latero-cortical Network

LFP – Local Field Potentials

mAchR – muscarinic Achetylcholine Receptor

M1 – Primary Motor area

M2 – Secondary Motor area

MRI – Magnetic Resonance Imaging

MUA – Multi-Unit Activity

NpHr – Halorhodopsin

Opto-fMRI – optogenetics Fmri combination

PFC – Prefrontal cortex

PolyTh – Polymodal Thalamus

Rs – Retrosplenial cortex

rsfMRI – Resting State fMRI

RSN – Resting State Network

SalB – Salvinorin B

SEM – Standard Error of the Mean

S1 – Primary Somato-sensory cortex

S2 – Secondary Somato-sensory cortex

TeA – Temporal Association area

Th – Thalamus

UniTh – Unimodal Thalamus

V1 – Visual cortex

1. Introduction

1. 1. Mapping brain-wide functional connectivity with resting-state fMRI

Functional Magnetic resonance imaging (fMRI) is increasingly widely used to probe functional synchronization in the resting brain (e.g. in the absence of an active task or stimulus). This approach typically implies the computation of statistical dependencies between spontaneous fluctuations in Blood Oxigenated Level Dependent (BOLD) signal across brain regions as an index of inter-regional communication or "Functional Connectivity" (FC, **Figure 1.1**) (Biswal et al., 1995; Fox and Raichle, 2007; Friston, 2011; van den Heuvel and Hulshoff Pol, 2010).

Several studies have revealed that regions with synchronized activity define a set of well-defined brain topographies, namely resting-state networks (RSNs) (Beckmann et al., 2005; Bullmore et al., 2009; Damoiseaux et al., 2006; Power et al., 2014; Shehzad et al., 2009; Yeo et al., 2011). RSNs comprise functionally-related regions involved in sensory and cognitive function (Visual, Somatomotor, Auditory, Frontoparietal, Attentional, Limbic as described by Yeo et al, 2011), as well distributed associative areas, such as a Default Mode Network (DMN), whose cognitive and processing functions remain debated. This latter network is of special interest due to its disproportionately high metabolic demand at rest (Buckner et al, 2008; Gusnard and Raichle, 2001; Raichle, 2015; Raichle et al, 2001; Uddin et al, 2009; Yeo et al, 2011). Interestingly, in 2005, Fox and colleagues showed that

the DMN is intrinsically anti-correlated to a latero-cortical network (LCN) termed “task-positive network”, composed by regions routinely activated during goal-directed task performance (Fox et al., 2005). This relationship reveals a possible antagonistic organization between these two key macro-systems of the human brain.

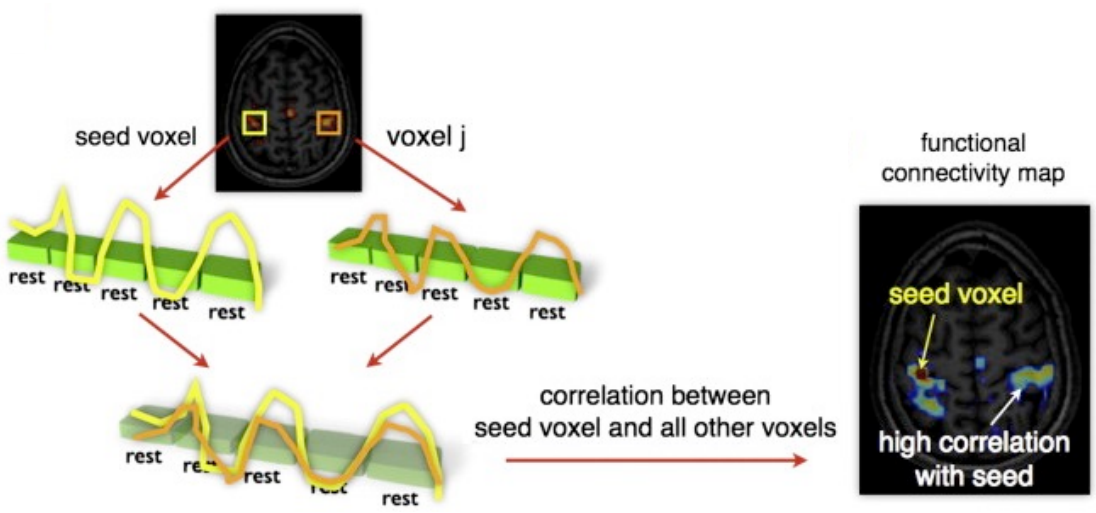

Figure 1.1 Resting-state fMRI measures the correlation between spontaneous fluctuations in BOLD activity as an index of functional connectivity. FC is often quantified with respect of a region of interest, termed seed region. A high correlation between BOLD fluctuations in the seed voxel and a voxel j is thought to reflecting high functional connectivity (i.e. synchronization) between these regions. This approach can be extended to map correlation across all the voxels of the brain with respect to the probed region, yielding a functional connectivity map (from van den Heuvel and Hulshoff Pol, 2010).

A popular way to conceptualize FC maps, is by mathematically describing them as graphs, comprising a set of nodes (neuronal areas) and edges (their interconnections). These representations offer the possibility of mapping and probing the “topology” of FC networks, i.e. their network structure. Within this framework, nodes appearing to exhibit an exceedingly high number of interregional connections are referred to as a hub nodes, a terminology reflecting the structure of real world networks such as airports or the whole wide web (Cavanna and Trimble, 2006; Hagmann et al., 2008). Several studies have been conducted on voxel- wise or region-wise FC graphs of the human brain, suggesting that associative cortical regions, such as the posterior and anterior cingulate cortex (precuneus) and the ventromedial frontal cortex, are configured as key integrative brain

hubs (Cole et al., 2010; Tomasi and Volkow, 2011). Owing to their prominent connectivity profile, it has also been suggested that these hub regions may represent points of potential vulnerability to dysfunction in brain disorders. Consistent with this notion, aberrant rsfMRI connectivity profiles have been described for several hub regions in pathological conditions such as autism spectrum disorder, schizophrenia and neurodegenerative disorders (Buckner et al., 2008; van den Heuvel and Sporns, 2013).

Altered rsfMRI connectivity is observed in major brain disorders

The study of large-scale brain connectivity networks may provide a key to understand brain disease. Prior studies involving rsfMRI have displayed widespread connectivity abnormalities in several brain disorders, encompassing hypo- or overconnectivity between widespread networks of brain regions **(Fig. 1.2).** For instance, reduced rsfMRI connectivity in associative cortical areas have been described in schizophrenia (Clinton and Meador-Woodruff, 2004; Friston and Frith, 1995; Garrity et al., 2007; Huang et al., 2010; Lynall et al., 2010; Marenco et al., 2011; Welsh et al., 2008) as well as Autism Spectrum Disorder (ASD, Just et al., 2006; Lynch et al., 2013). On the contrary, patients diagnosed with depression have been shown to exhibit increased resting-state activity in frontal and parietal components of the DMN, and in cortico-midline system (Wang et al., 2012). A prevalent feature of bipolar disorder appears to be reduced resting-state activity in prefrontal areas (Leichsenring et al., 2011; Lis et al., 2007).

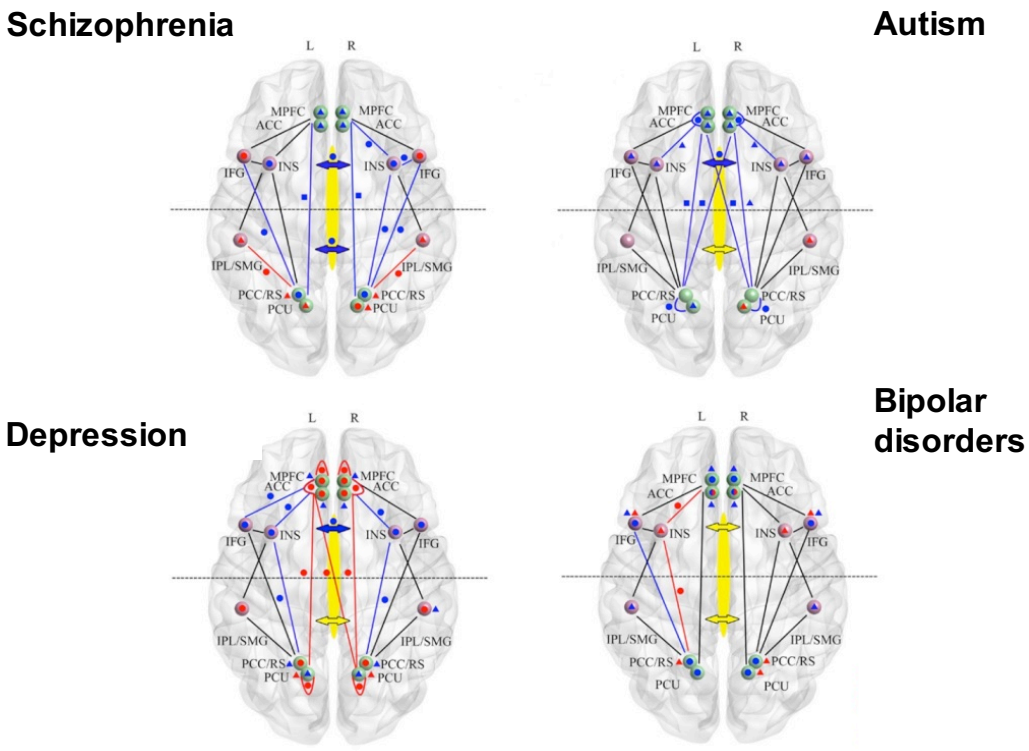

Figure 1.2 Aberrant functional connectivity in brain disorders. The figure shows different connectivity profiles of different pathologies (Zhao et al., 2013).

However, fundamental questions related to the etiopathological and biological foundations of these alterations remain to be addressed. For one, it is unclear what are the drivers of these aberrancies and what is their actual neurobiological significance. Importantly, many of these questions stem from the correlational nature of FC as inferred from rsfMRI. This problem is compounded by our inability to employ precise perturbational approaches required to disambiguate correlation-based measurements of functional coupling in humans.

More specifically, perturbational approaches are critically required for a deeper understanding of brain-wide rsfMRI coupling for two main reasons. First, the correlative nature of rsfMRI makes measures of functional connectivity fickle indicators of direct interareal interaction, as synchronous signals could reflect the contribution of global

fluctuations, or could be driven by spatially remote functional interactions with a third region. Second, a deeper understanding of the fundamental elements and dynamic rules underlying the establishment of rsfMRI coupling is required to reliably back-translate clinical alterations in rsfMRI connectivity into testable neurophysiological events and models that can help understand, diagnose or treat brain disorders.

It is now apparent that a full understanding of the origin and significance of coordinated macroscale functional connectivity and its aberrations requires interventional approaches and controlled experimental conditions which are only achievable with animal models (Gozzi and Schwarz, 2016).

1. 2. Mouse brain RSNs organization recapitulates key features of the primate and human brain

Cortical and subcortical RSNs that recapitulate neuroanatomical features of known functional systems of the human brain have been reliably detected in awake and anaesthetized primates (Rilling et al., 2007; Vincent et al., 2007) as well as rats (Hutchison et al, 2010; Lu et al, 2012; Schwarz et al, 2012, 2013). Towards the goal of understanding the basis of rsfMRI coupling, research in our lab has pioneered methods to map rsfMRI connectivity in simpler model organism amenable to sell-type specific neuromanipulations, such as the mouse **(Fig. 1.3).**

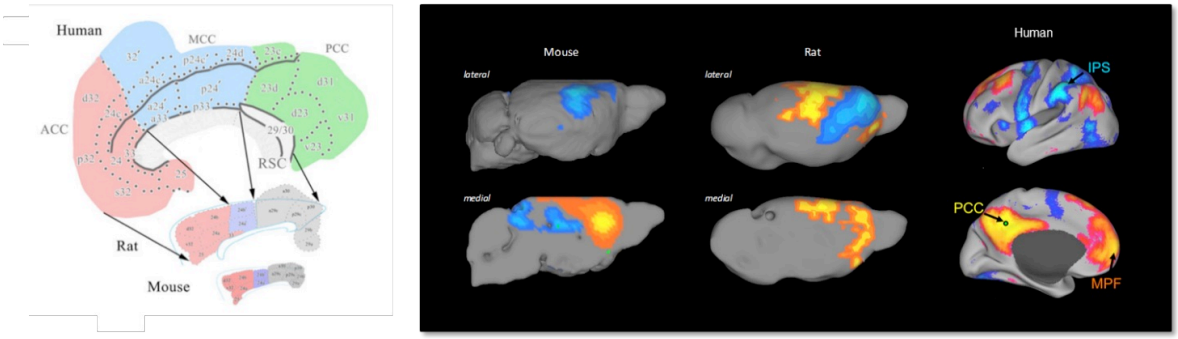

Figure 1.3 Mouse brain rsfMRI network organization recapitulates features observed in primates and human brain. This finding supports the idea that some structures are evolutionary conserved across species (Gozzi and Schwarz, 2016; Vogt and Paxinos, 2014).

In particular, Sforazzini and colleagues provided the first demonstration of the presence of robust distributed and homotopic rsfMRI connectivity networks in the mouse brain (Sforazzini *et al*, 2014). In the same study, a plausible mouse homologue of the human DMN was identified. Interestingly, the mouse DMN presents anti-correlated rsfMRI activity with a lateral network. The latter one comprises sensorimotor cortical areas and extends from the insular cortex to anterior motor areas, considered to represent frontal eye fields in the rodent (Sforazzini *et al*, 2014). These findings are in agreement with human investigations of the DMN, and replicate analogous results in primates (Buckner *et al*, 2008; Chai *et al*, 2012; Gozzi and Schwarz, 2015; Rilling *et al*, 2007; Vincent *et al*, 2007). In a subsequent study, Liska and colleagues described additional correspondences between human and rodent brain organization (Liska *et al*, 2015). Using a graph-theoretical approach, the authors identified the presence of six distinct functional modules related to known large-scale functional partitions of the brain. Including the DMN, as well as the LCN that exhibits putative features of a “task-positive” network in the mouse brain (**Fig. 1.4**). Importantly, consistent with human findings (Cole et al., 2010), the authors also described high strength connectivity nodes of the mouse brain to be located in the midline cingulate and prefrontal regions of the DMN. These results are in line with structural connectivity mapping in the mouse using axonal tracing (Stafford et al., 2014). Together,

the studies highlight the presence of evolutionary-conserved, mutually-interconnected functional hubs in the mouse brain (Liska *et al*, 2015, 2017; Liska and Gozzi, 2016), and support the translational validity of using of this species to investigate the neural basis of rsfMRI coupling.

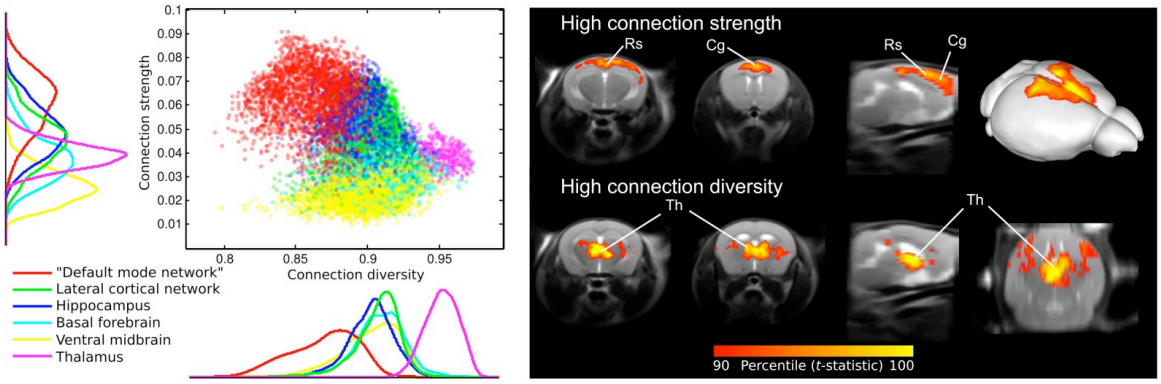

Figure 1.4 Global hubs of the mouse brain. On the left panel, connection diversity and connection strength values are plotted for all nodes in the average functional network. Nodes are color-coded according to their module. On the right black box (upper row), nodes surviving the top percentage threshold for connection strength are shown on two images in the coronal view (left), one image in the sagittal view (middle), and on a three-dimensional cortical surface rendering. In the lower row, nodes surviving the top percentage threshold for connection diversity are shown on two images in the coronal view, one image in the sagittal view (middle), and one image in the horizontal view (right) (from Liska et al, 2015).

Converging prefrontal hypoconnectivity in three unrelated mouse models of autism

An important recent development in the validation of rsfMRI in rodents has been the characterization of rsfMRI networks in disease models (Gozzi and Schwarz, 2015; Liska and Gozzi, 2016). rsfMRI measurements in transgenic rodent lines, where advanced genetic techniques allow manipulations of the genome and precise control of gene expression, represent a powerful tool to understand the neurobiological basis of connectivity alterations observed in human disease, bridging in this way an important translational gap (Gozzi and Schwarz, 2015; Liska and Gozzi, 2016). A powerful demonstration of the power of this apporach is the recent application of rsfMRI to probe the basis of FC alterations in mouse models recapitulating key ASD-related etiologies.

ASD is a range of developmental disorders characterized by deficits in social interaction and communication, and by restricted and repetitive behaviors (Durdon, 2008). Over the past decades, researchers identified an association between genetic factors and ASD (de la Torre-Ubieta et al., 2016) providing a platform to unravel the causal chain of events that results in ASD. Several studies have shown altered rsfMRI connectivity (both overconnectivity and underconnectivity) in adolescents, adults, and children with ASD (Gabrielsen et al., 2018). However, a key open question in this field is whether and how heterogeneous genetic forms of ASD might converge into circuital and behavioral alterations characteristic of this cluster of disorders. Towards this goal, a number of rsfMRI has been carried out in our lab to associated patterns of altered connectivity to specific ASD-related genetic etiologies.

In the first of such studies, the effect of homozygous loss-of-function mutations in *contactin associated protein-like 2* gene (CNTNAP2) on rsfMRI functional connectivity was described. This gene encodes a neurexin-related cell-adhesion molecule, and its mutation is strongly linked to ASD and epilepsy in consanguineous families (Rodenas-Cuadrado et al., 2014; Strauss et al., 2006). Loss of Cntnap2 in mice leads to abnormal neuronal migration, reduced number of GABAergic neurons, spontaneous seizures, and behavioral traits consistent with ASD symptoms in humans (Penagarikano et al., 2015). Using rsfMRI, Liska and associates showed that these phenotypes are associated with reduced local and long-range connectivity in prefrontal hub regions (Liska et al., 2015).Furthermore, fronto-posterior hypoconnectivity was found to be linked to impaired social behavior (Liska et al., 2015,**Fig. 1.5**), and a reduction in projecting neuron frequency was observed in the under-connected areas, implicating developmental miswiring as a plausible contributor of hypo-connectivity in these mice. Interestingly, common genetic variants in CNTNAP2 have been recently associated with similarly reduced prefrontal connectivity in humans (Scott-

Van Zeeland et al., 2010), hence establishing a plausible translational link between mouse and human findings. Collectively, this initial investigation of the effect of CNTNP2 mutations in rsfMRI connectivity revealed that ASD-associated mutations in this gene may predispose to neurodevelopmental disorders and ASD through dysregulation of macroscale functional network couplings and developmental miswiring.

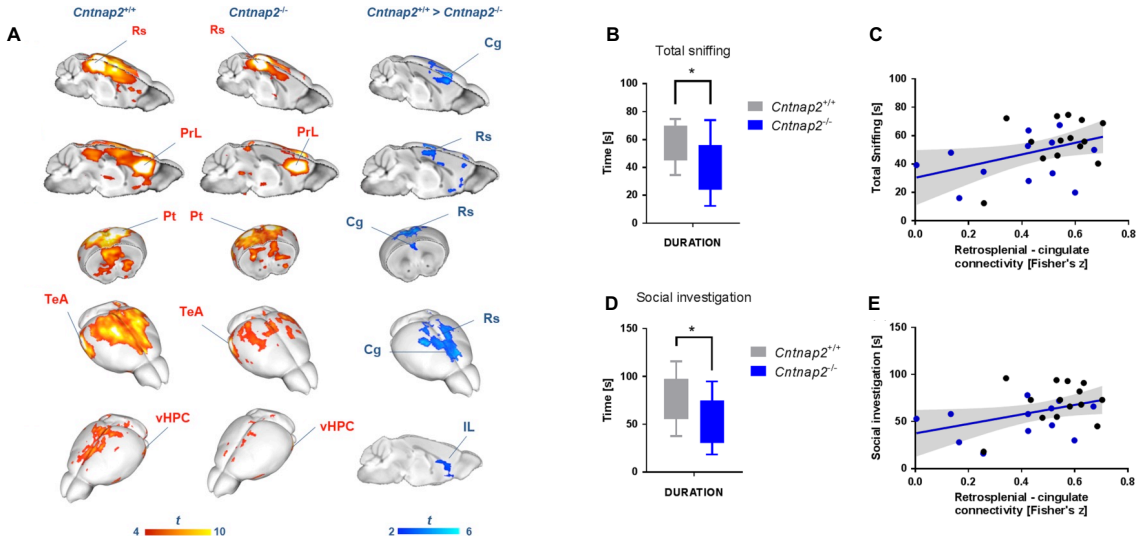

Figure 1.5 Reduced long-range connectivity in Cntnap2$^{-/-}$ mice. (A) Seed-correlation mapping highlighting convergent reduced connectivity between long-range cortical and subcortical regions as well as cingulate-prefrontal areas. Red/yellow shows areas with significant correlation with seed regions indicated in red text. Blue indicates foci of reduced connectivity in Cntnap2$^{-/-}$ mutants with respect to control mice. (B) Social behavior as measured by total sniffing duration (C) Association between retrosplenial-cingulate connectivity (VOI-to-VOI) and total sniffing duration. (D) Social behavior as measured by the duration of social investigation. (E) Association between retrosplenial-cingulate connectivity (VOI-to-VOI) and the duration of social investigation. *p < 0.05. Adapted from Liska et al., 2016.

Interestingly, similar rsfMRI findings were recently observed in two other models of autism. The first of these recent studies investigated the role of mutation in *SH3 and multiple ankyrin repeat domains 3* (Shank3), a leading cause of autism (Peca et al., 2011; Tabet et al., 2017)(Leblond et al., 2014). By using rsfMRI and behavioral recordings, Pagani and colleagues revealed that Shank3 deletion produces socio-communicative impairments via a focal dysregulation of prefrontal connectivity (Pagani et al., 2019). Specifically, the authors showed that homozygous loss of Shank3B results in disrupted fronto-cortical and fronto-striatal connectivity, an effect once again associated with short-range corticocortical

mis-wiring **(Fig. 1.6).** The same authors also documented that prefrontal connectivity deficits are tightly linked to socio-communicative impairments in a social interaction test.

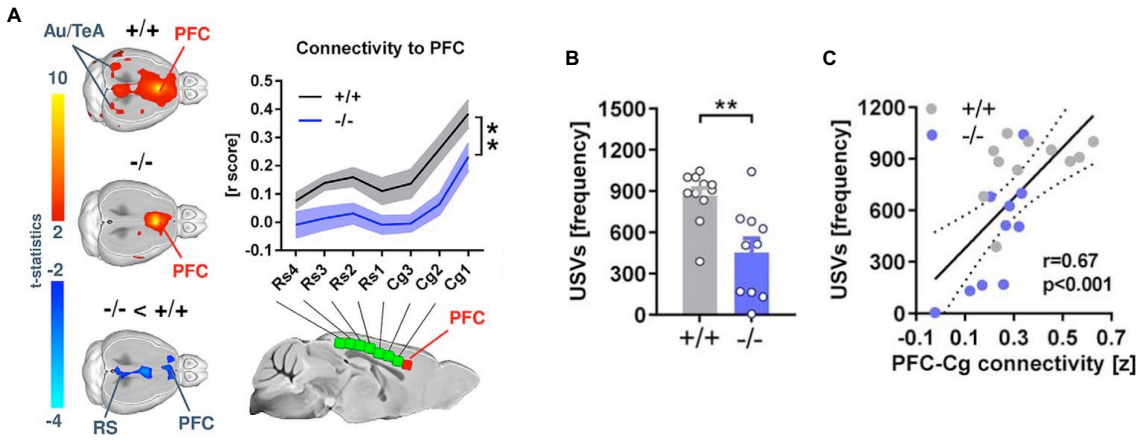

Figure 1.6 Prefrontal underconnectivity in Shank3B$^{-/-}$ mice. (A) Spatial extension of the regions exhibiting significant long-range connectivity with the PFC in Shank3B control (+/+, top) and mutant (-/-) mice. (B, C), Correlation between prefrontal connectivity and socio-communicative dysfunction. Cg, Cingulate cortex. *p 0.05, **p 0.01. Reproduced from Pagani et al., 2019, with permission.

A third recent study examined the role of chromosomal 16p11.2 deletion, one of the most common copy number variations in ASD and related neurodevelopmental disorders (Bertero et al., 2018). In a first of its kind example, this study directly compared rsfMRI connectivity in a mouse model and human population carrying the same genetic mutation. Using rsMRI data from the Simons Variation in Individuals Project (VIP) database (https://www.sfari.org), the authors showed that 16p11.2 deletion in humans carriers exhibit impaired analogous prefrontal connectivity, resulting in weaker long-range functional coupling with temporal-parietal regions. It was also documented that mice with the same genetic deficiency exhibited similarly diminished prefrontal connectivity, together with thalamo-prefrontal miswiring and reduced long-range functional synchronization. These results suggest that deletion in 16p11.2 may lead to impaired socio-cognitive function via dysregulation of prefrontal connectivity (Bertero et al., 2018, **Fig 1.7**).

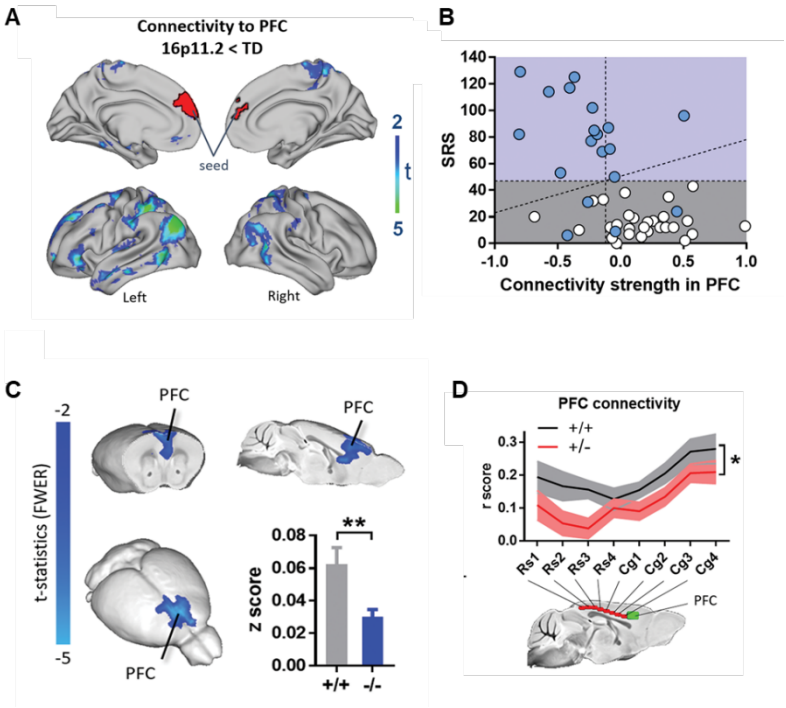

Figure 1 7. Cross-species prefrontal under-connectivity in 16p11.2 deletion(A) Targets of the PFC underconnectivity in human carries of 16p11.2 deletion, identified using seed-based analysis. (B) PFC connectivity strength in humans exhibited robust inverse correlation with SRS score ($r = -0.52$, $P < 0.001$). (C) Whole-brain voxel-wise mapping of global connectivity revealed reduced functional connectivity in the medial PFC of 16p11.2$^{+/-}$ mutant mice compared to control littermates ($P < 0.05$, cluster-corrected). (D) Connectivity profile between a series of midline seeds (Cg = cingulate cortex) and the PFC (green). Reproduced from Bertero et al., 2018, with permission.

Together, these findings suggest that unrelated genetic mutations associated with syndromic forms of ASD result in converging under-connectivity in the prefrontal cortex, and support a key stabilizing role of functional connectivity hubs in serving a key contribution as network stabilizers.

Prompted by these observations, my work was aimed to design a set of manipulations aimed to causally probe the neural drivers of these rsfMRI alterations. Specifically, given the prevailing view that rsfMRI connectivity is tightly constrained by underlying structural connectivity, I designed a set of manipulations aimed to silence the prefrontal cortex, under the assumption that reduced activity in the PFC, a key area of the mouse social brain, would underlie the observed underconnectivity and social impairments. In the following

chapter I will briefly described some of the tools that can be used in the mouse to regionally manipulate activity.

1. 3. Perturbational approaches to unravel rsfMRI connectivity

In 1979, in an outstandingly prescient article, Nobel laureate Francis Crick proposed a "wish list" of items that would be essential for understanding brain function:

"[F]or example, a method that would make it possible to inject one neuron with a substance that would then clearly stain all the neurons connected to it, and no others, would be invaluable. . . [Similarly,] a method by which all neurons of just one type could be inactivated, leaving the others more or less unaltered [is also needed]." (Crick, 1979)

In a later article, Crick also presaged the need for methods to "turn neurons on" (Crick, 1999). Recent developments in neuro-genetic and biophysics have brought about a set of tools that have made Crick's vision technically feasible. Specifically, optogenetics methods allow for temporal precise neuronal manipulation via expressions light responsive proteins (opsins) (Fenno et al, 2011). More recently, chemogenetics tools have been generated for sustained neuronal manipulations (Farrell and Roth, 2013). This method involves the expression of engineered receptor on targeted neurons, which can be activated by the administration of an exogenous, biologically inert ligand (Farrell and Roth, 2013; Sternson and Roth, 2014). The following paragraphs introduces both methods and their potential as perturbational tool in rsfMRI.

Optogenetics and opto-fMRI

Optogenetics refers to the expression of microbial opsin in a specific neuronal population. When illuminated with the appropriate wavelength, these opsins respond by firing within milliseconds, allowing tight temporal control of neuronal activity (**Fig 1.9**). According to the type of opsin, the response could involve either depolarization or hyperpolarization of cell membranes, resulting in excitation and inhibition of neuronal activity, respectively (Galvan et al., 2018). The most common excitatory tools (i.e., depolarizing opsins) include variants of the cation channel channelrhodopsin (ChR) (Boyden et al., 2005; Nagel et al., 2005), while commonly used hyperpolarizing opsins are proton or chloride pumps, such as archaerodopsin (Arch, Chow *et al*, 2010) and halorohodopsin (NpHR, Gradinaru *et al*, 2008).

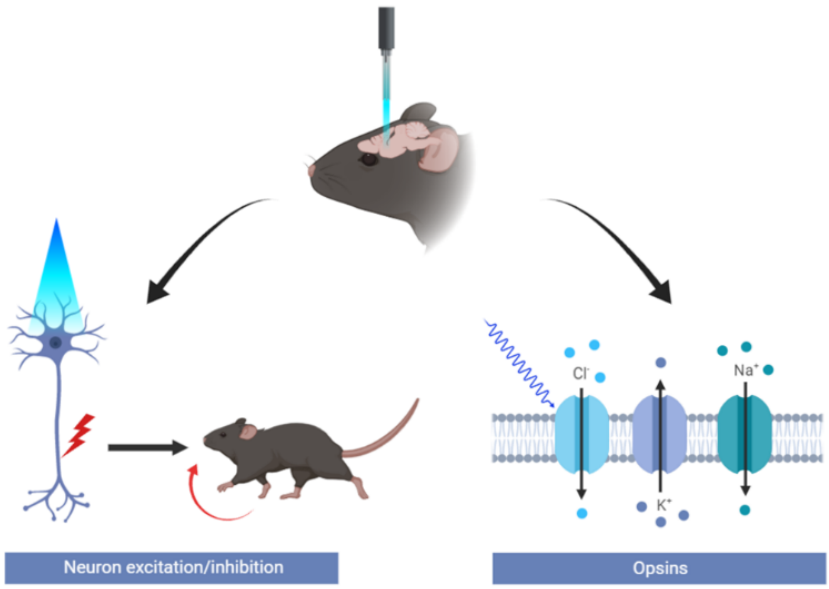

Figure 1 8. Optogenetics. Different kinds of opsins are now available and can be expressed in specific neuronal populations. When illuminated with the appropriate wavelength, these opsins respond by firing within milliseconds, allowing tight temporal control of neuronal activity.

The presence of different types of opsins, regulating different signaling cascade, offers the opportunity to manipulate different populations of neurons at precise times. A notable

example of this approach, highly relevant for the present project, has been described by Yizhar and colleagues in 2011, who used optogenetics to independently manipulate the activity of excitatory pyramidal neurons and inhibitory parvalbumin (PV) interneurons within the mouse prefrontal cortex (PFC) during a social exploration task (Yizhar et al., 2011b). The authors showed that increasing the excitatory/inhibitory (E/I) balance by stimulating pyramidal neurons in the PFC abolished social exploration and disrupted social preference in the three-chamber test. The detrimental effect of increased excitation was ameliorated by simultaneously stimulating PV interneurons, showing that an appropriate E/I ratio in the PFC is required for social motivation in mice. These findings have been linked to human literature postulating a role for altered E/I balance within the PFC in psychiatric disorders including schizophrenia and autism (Toro et al., 2010).

From a methodological standpoint optogenetics requires:

- Engineered control tools that can be readily targeted to specific cells, typically in combination with a conditional expression system, such as the Cre-recombinase/LoxP system or viral injection.
- Technologies for light delivery.
- Methods for integrating optical control with compatible readouts (such as fluorescent organic or genetically encoded activity indicators, electrical recording, fMRI signals, or quantitative behavior analysis).

Combining optogenetics manipulation with fMRI, an approached termed opto-fMRI (Lee, 2012), enables specific stimulation of precise circuit elements with non-invasive monitoring of the global network response. Opto-fMRI can reveal how the activity of specific neuronal populations impacts the function of the brain. The first published opto-fMRI study (Lee et al., 2010) demonstrated some of the basic principles regarding the capabilities of this

method. Specifically, the authors stimulated excitatory neurons in the motor cortex of rodents, eliciting positive BOLD signals at the stimulus location, in turn causing a robust thalamic activity (long-range connection). Furthermore, they showed that opto-fMRI allows to visualize the causal effect of specific cell types defined not only by genetic identity and cell body location, but also by axonal projection target. Liang and colleagues more recently used opto-fMRI to reveal the functional network that is activated by the PFC in rodents (Liang et al., 2015). The authors showed that expression of ChR2 in the rat PFC coincided with robust BOLD activation of the PFC, striatal and limbic regions which are anatomically connected to the PFC.

Together, these initial studies provide a proof-of-concept demonstration of the feasibility of employing opto-fMRI for functional circuit analysis as well as global phenotyping of dysfunctional circuitry. Importantly, this tool enables bridging scales by linking neuronal function and anatomy from single cell to circuit level. The use of opto-fMRI in combination with rsfMRI may provide important insight into the neural determinants of rsfMRI BOLD connectivity, and bridge an important gap related to the specific cellular mechanisms underlying BOLD signal correlations.

Chemogenetic and chemo-fMRI

Chemogenetics techniques use the expression of engineered muscarinic acetylcoline receptors (mAchR) into a specific cell population, which can be modulated by systemically administered an exogenous ligand that is otherwise biologically inert (Farrell and Roth, 2013; Sternson and Roth, 2014).

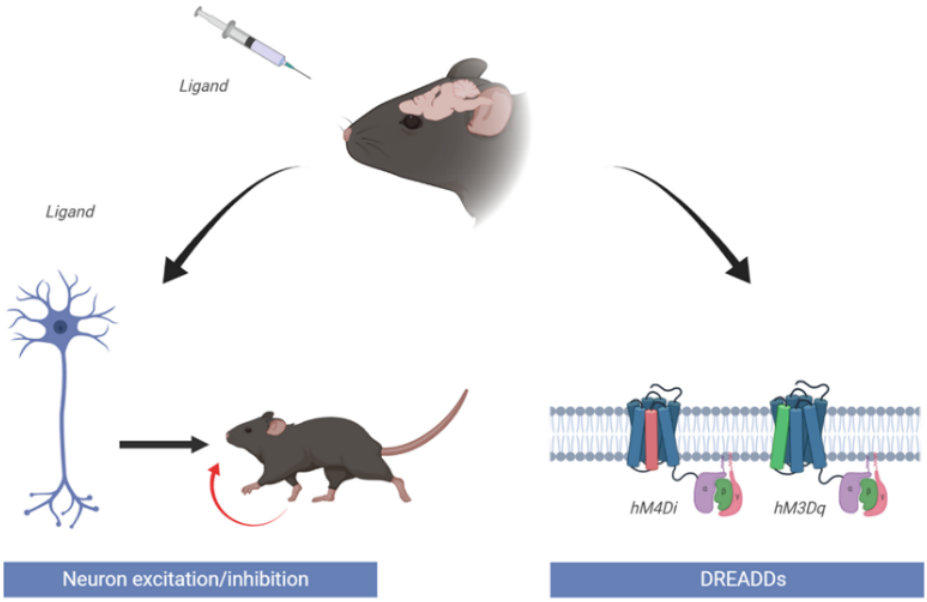

Figure 1 9 Chemogenetics. Different kinds of DREADDs can be expressed in specific neuronal populations. The peripheral administration of a ligand leads to receptor activation, triggering an intracellular signaling cascade that can enhance or inhibit neuronal activity.

The most widely used chemogenetics technique (**Fig1. 10**) relies on the expression of designer receptors exclusively activated by designer drugs (DREADDs) in neurons. DREADDS are maximally responsive to clozapine-N-oxide (CNO), a metabolite of the antipsychotic drug clozapine (Roth et al., 1994). CNO is a small molecule that can rapidly diffuse in the central nervous system by crossing the blood-brain barrier with a long-term residence (>60 min). In addition, it is bioavailable (Bender et al., 1994) and is pharmacologically selective (<1μM affinity at the native muscarinic receptors; Armbruster *et al*, 2007). Furthermore, because its parent compound clozapine has high affinity at the native muscarinic receptors, only a limited number of mutations were supposed to be required to make them highly responsive to CNO. To generate them, the native receptors have been engineered through cyclic procedures of random mutagenesis and screening, in order to create and select receptors that had maximally lost their natural affinity to acetylcholine (Ach) and that were maximally responsive to inert ligand. Depending on the

interacting G-protein, two main classes of DREADDs have been developed: Gq-coupled (hM3Dq) and Gi-coupled (hM4Di) DREADDs. Ligand-mediated activation of hM3Dq leads to intracellular Gq-mediated signaling cascade, leading to enhance neuronal firing. Gi-DREADDs promote Gi-protein-dependent intracellular signaling, thereby inducing neuronal activity inhibition. Furthermore, a novel class of inhibitory DREADD has been recently generated from κ-opioid receptor (KOR). The so-called KORD (KOR-DREADD) is responsive to salvinorin B (SalB), an otherwise inert molecule, and not-responsive to the endogenous ligand, the opioid peptide dynorphin. Owing to these properties, KORDs can be expressed simultaneously with excitatory Gq-DREADDs for the sequential chemogenetics activation and inhibition of neuronal populations (Vardy et al., 2015).

As discussed above for optogenetics, the combination of chemogenetics and fMRI represents a novel experimental strategy that may permit to bridge different levels of inquiry in experimental neuroscience. A first demonstration of this approach was reported by Giorgi and colleagues in 2017, who coined the term “chemo-fMRI” to refer to the combined use of fMRI and chemogenetics. The authors of this work used chemo-fMRI to causally probe the brain-wide substrates modulated by endogenous serotonergic activity (Giorgi et al., 2017a) via the use of DREADD receptors. They showed that endogenous stimulation of serotonin-producing neurons does not affect global brain activity but results in region-specific activation of a set of primary target regions encompassing cortico-hippocampal and ventral striatal areas. The results of Giorgi et al, identify the primary functional targets of endogenous serotonergic stimulation and establish causation between activation of serotonergic neurons and regional fMRI signals. From a methodological standpoint, this work paves the way to the combined use of chemogenetics and fMRI to unravel the large-scale substrates modulated by specific neuronal populations in the living mouse brain (Giorgi et al., 2017).

The impact of the perturbation on global network organization using resting-state fMRI functional connectivity measures, given by ligand-DREADDs activation, was recently reported in another recent study conducted on rhesus monkey (Grayson et al., 2016). The authors pharmaco-genetically inactivated the amygdala in rhesus monkeys while performing rsfMRI measurements. Amygdala inactivation disrupted amygdalo-cortical communication and distributed cortico-cortical coupling across multiple functional brain systems. This work shows that damage to a single small functional area could have widespread consequences across the whole brain and highlights the power of combining a focal DREADD manipulation with rsfMRI to identify changes in local and global network organization in vivo.

Optogenetics vs. Chemogenetics

Opto-fMRI and chemo-fMRI provide straightforward and widely applicable opportunities to elucidate relationships between local neuronal activity and global network activity in a controllable manner, which will increase our understanding of the functioning and dysfunctioning of large-scale neuronal networks from rsfMRI measurements in health and disease. While these tools have enabled the functional and behavioral dissection of many discrete brain circuits with exquisite precision (Yizhar et al., 2011a) a number of key methodological divergences between these two set of tools set them apart. Optogenetic provides precise spatial (subcellular) and temporal (microsecond) control of signaling. However, this method requires invasive implants of optic fibers and expensive laser equipment that make its combination with fMRI technically challenging. On the other hand, chemogenetics approaches are generally more easily implemented, for they are less invasive (they do not require the implantation of probes, or dedicated equipment), and CNO diffuses widely following administration, allowing the modulation of signaling and activity in distributed neuronal populations over prolonged time windows (e.g. 1 hour or

so) that are especially suited to the generation of steady brain states amenable to rsfMRI imaging. While DREADD's lack of precise temporal control can be problematic for behavioral studies, this aspect does not appear to be an issue in imaging studies of rsfMRI activity, a neural mass phenomenon that benefits from the modulation of larger brain areas achievable with chemogenetics approaches.

A noteworthy disadvantage of chemogenetics is the possible in vivo back-conversion of CNO into clozapine (Gomez et al., 2017). While this effect can result in unspecific effects, tight control of CNO dosing (Giorgi et al., 2017), or the use of clozapine microdosing (Zerbi et al., 2019) can be used to minimize these contributions. It is however important to consider that an accurate control of these effects requires the experimental use of a specific control group in which the baseline effect of the selected dose of DREADD actuator is rigorously assessed.

In summary, chemogenetics and optogenetics tools differ in their feasibility and spatiotemporal resolution. However, chemo-fMRI appears to be more suited to investigation of rsfMRI connectivity owing to its ability to measure the influence of specific circuits on network organization over a prolonged time window, with lower invasiveness, and without the restriction of chronic implants or the complications arising from lesion-induced compensatory changes.

2. Aim of this work

The initial aim of this project was to propose a possible link between neuronal activity and the connectivity phenotype found in several mutations associated with ASD: is this abnormal connectivity profile due by the inhibition of the neuronal activity at the level of specific brain regions as dictated by prevailing interpretation of rsfMRI functional connectivity?

Importantly, the possibility of implementing neural silencing during rsfMRI scanning also offered us the chance to experimentally validate structurally based models of functional connectivity. The observation of a paradoxical increase in rsfMRI connectivity upon neural silencing of the PFC led us to further investigate the basis of this phenomenon using two orthogonal neural manipulations. Specifically, we implemented an extended chronic silencing using a virally-mediated overexpression of a potassium channel, followed by a set of mechanistic investigations via the used of DREADD chemo-fMRI. By using these converging approaches, we obtained a set of unexpected results that advance our understanding of the neural basis of rsfMRI functional coupling, and that might facilitate their back-translation of functional over-connectivity in human brain disorders. A detailed description of our approach and experimental findings is reported in the following chapter.

.

3. Paradoxical fMRI overconnectivity upon chemogenetics silencing of the mouse prefrontal cortex

This Chapter will be published as:

"Cortical silencing results in fMRI over-connectivity." Carola Canella, Federico Rocchi, Shahryar Noei, Daniel Gutierrez-Barragan, Ludovico Coletta, Alberto Galbusera, Massimo Pasqualetti, Giuliano Iurilli, Stefano Panzeri, Alessandro Gozzi. Biorxiv, 2020.

3. 1. Background and Introduction

A rapidly expanding approach to understand neural organization is to map large-scale patterns of spontaneous neural activity in the resting brain via non-invasive neuroimaging methods. The prevalence and robustness of resting state fMRI (rsfMRI) have promoted the widespread use of this approach, leading to the observation that spatio-temporal patterns of spontaneous fMRI activity are organized into highly coherent functional networks, defined by temporally correlated fluctuations in BOLD signal (Power et al., 2014). The non-invasive nature of rsfMRI has fueled the use of this method to map intrinsic brain network organization in the healthy human brain, as well as in clinical populations diagnosed with psychiatric or neurological conditions in which evidence of disrupted or aberrant rsfMRI functional coupling has been largely documented (Fitzsimmons et al., 2013; Hull et al., 2017). However, despite the growing popularity of rsfMRI, our knowledge of the underpinnings and neural drivers of brain-wide fMRI coupling remains very limited.

Statistical dependencies in spontaneous fMRI signal are commonly interpreted as an index of interareal axonal communication and functional connectivity (Power et al., 2014). Based on the Hebbian construct that neurons that fire together wire together (Lowel and Singer, 1992), this interpretative framework is supported by computational and empirical evidence suggesting that structural and rsfMRI-based connectivity are robustly related. For example, structural and functional connection strengths are correlated both at the whole-brain and mesoscopic scale (Hagmann et al., 2008; Wang et al., 2013; Coletta et al., 2020a), and rsfMRI network topography closely recapitulates patterns of anatomical connectivity (Honey et al., 2009; Goni et al., 2014). Computational modelling supports this view, as synchronous rsfMRI fluctuations can be modelled via the intersection of dynamic processes and reciprocal long-range axonal interactions (Ponce-Alvarez et al., 2015), and simulated axonal lesions result in

reduced functional coupling (Alstott et al., 2009). In keeping with this, experimental resection of callosal connections (O'Reilly et al., 2013) and neural inactivation of the amygdala have been shown to reduce functional connectivity with regions anatomically linked to the manipulated areas (Grayson et al., 2016). However, despite the prominent body of research supporting prevailing structurally-based interpretations of rsfMRI connectivity, evidence arguing against a dyadic relationship between structural and rsfMRI connectivity has also been reported. For example, robust rsfMRI coupling among brain regions not directly structurally connected has been reported in humans, primates and rodents (Tyszka et al., 2011; O'Reilly et al., 2013; Sforazzini et al., 2016). Similarly, clinical investigations of neurological disorders encompassing a physical disruption or inactivation of cortical areas (e.g. Parkinson's disease, multiple sclerosis or stroke) have often been found to be associated with paradoxically increased interareal rsfMRI connectivity (Hillary and Grafman, 2017), arguing against a strictly monotonic relationship between structural and functional connectivity. These observations suggest that global synchronizing mechanisms could contribute to brain-wide rsfMRI coupling, and call for a deeper investigation of the causal role of axonal connectivity in shaping large-scale functional connectivity.

Perturbational approaches are critically required to disentangle the neural drivers of brain-wide rsfMRI coupling for two main reasons. First, the correlative nature of rsfMRI makes measures of functional connectivity ambiguous indicators of direct interareal interaction, as synchronous signals could reflect the contribution of generalized slow fluctuations, or could be driven by spatially remote functional interactions. Second, targeted deconstructions of the fundamental elements governing rsfMRI coupling could uncover the cause-effect nature of patterns of rsfMRI dysconnectivity associated with brain pathologies, enabling a back-translation of dysconnectivity into interpretable neurophysiological events and models that can

help understand, diagnose or treat brain disorders. Here we combine rsfMRI, viral or chemogenetic manipulations (chemo-fMRI, Giorgi et al., 2016) and in vivo electrophysiology to probe how inactivation of cortical activity causally affects rsfMRI coupling. Surprisingly, we find that chronic and acute neural silencing of the mouse medial prefrontal cortex (PFC) results in paradoxical functional rsfMRI *overconnectivity* between the silenced area and its thalamo-cortical terminals, an effect associated with decreased gamma activity in the targeted regions, and increased delta band neural coherence between overconnected areas. Our findings suggest that rsfMRI coupling does not monotonically reflect reciprocal inter-areal communication under all conditions, and reveal a critical contribution of global rhythm generators to the establishment of brain-wide functional coupling.

2. Experimental procedures

Ethical statement

All in vivo experiments were conducted in accordance with the Italian law (DL 26/214, EU 63/2010, Ministero della Sanità, Roma). Animal research protocols were reviewed and consented by the animal care committee of the University of Trento and Italian Ministry of Health (authorization no. 852/17 to A.G.). All surgical procedures were performed under anesthesia.

Animals

Adult (6 weeks old) male C57Bl6/J were purchased from Jackson Laboratories (Bar Harbor, ME, USA). Mice were housed with temperature maintained at 21 ± 1°C and humidity at 60 ± 10%.

Definition of PFC

Our anatomical definition of mouse PFC reflects recent neuroanatomical (Carlén, 2017) and cytoarchitectural cross-species comparisons (Vogt and Paxinos, 2014), according to which the mouse PFC comprises a prelimbic region, corresponding to primate Brodmann area 32 (A32), the anterior cingulate cortex, corresponding to Brodmann area A24b, and the infralimbic cortex, corresponding to Brodmann area A24a. Our viral manipulations were therefore aimed to silence an anatomical ensemble comprising all the above mentioned regions at the following coordinates, expressed in millimeter from Bregma: 1.7 from anterior to posterior, 0.3 lateral, −1.7 deep (Paxinos and Franklin, 2003).

Viral injections

Mice were anesthetized with isoflurane and head-fixed in a stereotaxic apparatus (Stoelting). Injections were performed with a Hamilton syringe mounted on Nanoliter Syringe Pump with controller (KD Scientific), at a speed of 0.05 μl/min, followed by a 5–10 min waiting period, to avoid backflow of viral solution. The following injections volumes were employed: 300 nL (AAV8-hSyn-hM4D(Gi)-mCherry and AAV8-hSyn-GFP; http://www.addgene.org) or 2 μL (AAV8-hSyn-MYC-mKir2.1(E224G/Y242F)-IRES-GFP, (Xue et al., 2014), http://www.vectorbiolabs.com or AAV8-hSyn-GFP; http://www.addgene.org) of viral suspension were injected bilaterally in the mouse PFC (see coordinates above). rsfMRI or electrophysiological recordings were carried out no sooner than three weeks after the injection, to allow for maximal viral expression.

RsfMRI acquisitions

The animal preparation protocol was recently described in detail (Ferrari et al., 2012; Sforazzini et al., 2014; Gutierrez-Barragan et al., 2019). Briefly, mice were anesthetized

with isoflurane (5%, induction), intubated and artificially ventilated (2%, surgery). The left femoral artery was cannulated for continuous blood pressure monitoring and. At the end of surgery, isoflurane was discontinued and substituted with a shallow halothane regimen (0.75%) to obtain light sedation and to preserve cerebral blood flow auto-regulation (Gozzi et al., 2007). Ventilation parameters were adjusted to maintain normo-physiological paCO2 (< 40 mmHg) and paO2 levels (> 90 mmHg, corresponding to >98% hemoglobin saturation).

rsfMRI data acquisition commenced 30 min after isoflurane cessation. Functional images were acquired with a 7T MRI scanner (Bruker, Biospin) as previously described (Liska et al., 2015), using a 72 mm birdcage transmit coil and a 4-channel solenoid coil for signal reception. Single-shot BOLD rsfMRI time series were acquired using an EPI sequence with the following parameters: TR/TE 1000/15 ms, flip angle 60°, matrix 98 x 98, FOV 2,3 x 2,3 cm, 18 coronal slices, slice thickness 550 µm.

rsfMRI acquisition with Kir2.1-transduced (AAV8-hSyn-MYC-mKir2.1(E224G/Y242F)-IRES-GFP, n = 16) and control mice (AAV8-hSyn-GFP, n = 19) encompassed 35 minutes long timeseries, corresponding to 2100 volumes.

Chemo-fMRI acquisitions comprised two consecutive rsfMRI timeseries, encompassing 1800 volumes (30 min) and 2100 volumes (35 min), respectively. CNO (2 mg/kg, Sigma Aldrich) was injected intravenously fifteen minutes (volume #900) after the start of the first scan. The first 900 fMRI volumes of this first timeseries scan were used as pre-CNO baseline rsfMRI reference in timeprofile analyses. Based on the pharmacokinetic profile of CNO, the post CNO window was split into temporal domains as follows: the first 15 min post injection (900 timepoints) were considered part of a drug equilibration window, while the following 35 min (2100 timepoints) were considered to cover the DREADD active time window (“active”). All group comparison in the chemo-fMRI study were carried out within this latter time window,

unless otherwise stated. After post-mortem analyses of viral expressions, a total of N = 15 hM4Di and N= 19 GFP-transduced animals were retained for analyses.

Image preprocessing and analysis

Raw rsfMRI timeseries were preprocessed as described in previous work (Sforazzini et al., 2014; Gutierrez-Barragan et al., 2019). The initial 120 volumes of the time series were removed to allow for gradient equilibration effects. Data were then despiked, motion corrected and spatially registered to a common reference template. Motion traces of head realignment parameters (3 translations + 3 rotations) and mean ventricular signal (corresponding to the averaged BOLD signal within a reference ventricular mask) were used as nuisance covariates and regressed out from each time course. All rsfMRI time series also underwent band-pass filtering to a frequency window of 0.01–0.1 Hz and spatial smoothing with a full width at half maximum of 0.6 mm.

rsfMRI connectivity of the mouse DMN in Kir2.1 and chemo-fMRI scans was probed using a seed-based approach. In the case of the chemo-fMRI study, this quantification was carried out during the “active” time window. A 6 x 6 x 2 seed region was selected to cover the PFC areas targeted by viral injections. Voxel-wise intergroup differences in seed-based mapping were assessed using a 2-tailed Student's t-test ($|t| > 2$, $p < 0.05$) and family-wise error (FWE) cluster-corrected using a cluster threshold of $p = 0.05$ as implemented in FSL. The antero-posterior connectivity profile of the DMN was assessed by computing Person correlation between the PFC seed abovementioned an a series of 6 x 6 x 2 voxel seeds placed along the midline extension of the cingulate and retrosplenial cortices as previously described (Pagani et al., 2019). Quantification of cortico-thalamic connectivity was carried out with respect to a meta-regional parcellation of the cortical mantle in volumes-of-interest – VOIs, **Fig. S3.6**.

To rule out a possible confounding contribution of spurious neurovascular changes in CNO-induced rsfMRI connectivity alterations, we calculated and statistically compared the characteristic hemodynamic response function between kir2.1 and control mice, and between hM4Di-expressing and control mice upon CNO-administration (active phase), as previously described (Wu et al., 2013; Pagani et al., 2019).

To relate the strength of underlying anatomical connectivity to the regions exhibiting increased rsfMRI connectivity with voxel resolution we extracted outgoing projections from the affected PFC regions using a spatially-resampled (200 μm^3) version of a voxel scale model of the Allen Brain Institute structural connectome (Knox et al., 2018; Coletta et al., 2020). We then plotted the strength of PFC-departing structural projections against the corresponding between group difference in rsfMRI connectivity using the cluster corrected difference map, and assessed differences in the distribution of overconnected areas with respect to all the brain voxels using a Wilcoxon rank sum test.

To quantify the contribution of distinct thalamic subregions to overall group differences, we used k-mean clustering to partition voxels within thalamus based on whole-brain rsfMRI group-difference obtained using the PFC seed as recently described (Arthur and Vassilvitskii, 2007; Schleifer et al., 2019). To evaluate the optimal number of clusters across these solutions, the within-cluster sum of squared distances was heuristically compared via the elbow method. This approach revealed two major thalamic clusters, one medial and one bilateral partition encompassing sensory areas. Seed-based functional connectivity was subsequently computed for each of the two-resultant k-means clusters independently and the resulting functional connectivity maps compared and quantified across cortical VOIs.

Immunoistochemistry

Anesthetized mice were transcardially perfused with 4% PFA, brains were dissected, post-fixed over night at 4 °C, and sectioned in 40 μM thick slices using a vibratome (Leica Microsystems). Free-floating sections were incubated at 4°C overnight with rabbit anti-mCherry (ab213511, Abcam, 1:1000) or chicken anti-GFP (ab13970, Abcam, 1:1000). Sections were then incubated with goat anti-rabbit (Alexa Fluor 568, Invitrogen, 1:500) and anti-chicken (Alexa Fluor 488, Invitrogen, 1:500). Images were performed with MacroFluo microscope (Leica). Heat maps showing a regional quantification of viral expression were generated by co-registering slices to a common template space and manually delineating the regional distribution of viral expression in the targeted area. The binarized images were then averaged across groups to obtain a frequency map.

Electrophysiology acquisition

Electrophysiological recordings were carried out in animals subjected to the same animal preparation and sedation regime employed for rsfMRI mapping (Ferrari *et al*, 2012; Sforazzini *et al*, 2014). Briefly, mice were anaesthetized with isoflurane (5% induction), intubated, artificially ventilated (2% maintenance), and head-fixed in a stereotaxic apparatus (Stoelting). The tail vein was cannulated for CNO injection. To ensure maximal consistency between viral injections and recording site, the skull surface was exposed and an insertion hole in the right PFC was gently drilled through the skull corresponding to the location of prior viral injection point. A single shank electrode (Neuronexus, USA, interelectrode spacing 1 - 2.5 mm) was next inserted through the overlying dura mater by a microdrive array system (Kopf Instruments, Germany) at an insertion rate of 1 μm/min to reach the same stereotaxic coordinates employed for viral injection.

The site receptive fields were plotted manually and the position and size of each field were stored together the acquisition data. After electrode insertion, isoflurane was discontinued and replaced by halothane at a maintenance level of 0.75%, to induce rsfMRI-comparable sedation. Electrophysiological data acquisition commenced 1 hour after isoflurane cessation. Such transition time was required to ensure complete washout of isoflurane anesthesia and avoid residual burst-suppressing activity associated with extended exposure to deep anesthetic levels.

Neural activity was next recorded in consecutive 5 min time bins to cover a 15 min pre-injection time window, and a 60 min post CNO time-frame in n =5 hM4Di and n = 5 GFP-expressing mice. Signals were amplified using an RHD 2000 amplifier system (Intan Technologies). In the case of control Kir2.1 recordings, a four shank electrode was inserted along the coronal plane to bi-hemispherically cover the right (Kir2.1-expressing) and left (GFP-expressing) PFC (n = 4). The left region served as internal reference control to better assess the efficacy of Kir2.1 silencing. Electrophysiological signals were then recorded into 5 min time bins to cover a 35 min time-window.

To measure multi-electrode coherence, three electrodes were inserted in key anatomical substrates identified as overconnected in our chemo-fMRI mapping. A multi-probe micromanipulator (New-Scale Technologies) was used to insert a 32 channels four shank electrode (Neuronexus, USA, interelectrode spacing 1 - 2.5 mm) in the right prefrontal cortex, and two 16 channels single shank electrode (Neuronexus, USA, interelectrode spacing 1 - 2.5 mm) in the right medio-dorsal thalamus and retro splenial cortex, respectively To reduce tissue damage, an insertion insertion rate < 1 µm/min ws employed, allowing for a 30 minute equilibration every 400 µm traveled. To keep constant between electrodes the reference signal we fixed together the ground electrodes and put them in contact with the cerebral brain fluid

through a window drilled in the skull. Signals were then recorded into 1 min time bins to cover a 15-min pre-injection baseline and a 40-min post CNO time window in n = 5 hM4Di and n = 5 GFP-expressing adult C57Bl6/J mice.

Local Field Potential (LFP) and multi-unit activity (MUA)

To compute LFP signal, raw recordings were first down-sampled to 4 kHz, then band-pass filtered to 1-250 Hz. A two-step filtering procedure was employed as previously described (Belitski et al., 2008). Briefly, raw timeseries were first low-pass filtered using a 4^{th} order Butterworth filter with cut-off frequency of 1 kHz. The resulting timeseries were next down-sampled to 2 kHz, to be again filtered using a Kaiser window filter between 1Hz to 250Hz (with a sharp transition bandwidth of 1Hz, passband ripple of 0.01 dB and a stop band attenuation of 60 dB) and then resampled at 1 kHz. All the filtering was applied both in forward and backward temporal direction to avoid any phase transitions due to filtering.

To compute multi-unity activity (MUA), the raw PFC recordings were first high-pass filtered using a 4^{th} order Butterworth filter with a <100 Hz cut off frequency, then band-pass filtered between 400 and 3000 Hz using a Kaiser window filter (with transition band of 50 Hz, stopband attenuation of 60 dB, and passband ripple of 0.01 dB). The absolute value of the obtained signals was then down sampled to 4 KHz and low-pass filtered at 250 Hz, to be next down-sampled to 1 KHz to match the sampling rate of the LFP (Belitski et al., 2008). The MUA index obtained with this procedure is believed to be sensitive to neural activity within an area of ~140–300 μm around the electrode tip (Logothetis et al., 2001). A spike detection threshold corresponding to 4-times the median of the high-passed signal between 400 and 3000 Hz was employed. The resulting value was divided by 0.6745 as per the procedure suggested by Quiroga and associates (Quiroga *et al*, 2004). Moreover, to account for the natural refractory

time of neuronal activity, spikes were considered to be biologically plausible and as such retained in these computations only if occurring more than 1 ms apart.

To quantify effectiveness of Kir2*.1* in suppressing spontaneous activity, firing rate was estimated by dividing the number of spikes per electrode by the recording duration in seconds. The resulting spike rates were averaged across the channels corresponding to the virally targeted or control region. The average spike rate for four subjects were next tested against each other using paired student t-test. To assess the effect of chemo-fMRI manipulations, spiking activity was computed in hM4Di and GFP-expressing mice as described above and segmented into one-minute bins. We next computed the channel averaged firing rate for each segment, and normalized this value with respect to the firing rate recorded during baseline (pre-CNO) period. The resulting baseline normalized firing rate index was then used to assess changes in spiking rate upon CNO injection in the two experimental cohorts.

To obtain a time-resolved statistical assessment of the effect of chemogenetic silencing, we computed for each subject the autocorrelation of the channel-averaged firing rate for each subject, and next assessed the time lag necessary for the autocorrelation function to drop below a (95%) confidence interval. We next resampled for each subject the original baseline-normalized firing rate trace over time according to the obtained lag times, and split the time window into three different periods: 0 to 15 minutes (transient time), 15 to 35 minutes and 35 to 55 minutes after CNO the injection (active times). We pooled all the remaining data points in these windows both over time and over subjects and then compared the median between the two populations using two-sided Wilcoxon rank-sum test. The obtained p-values were corrected using Bonferroni-Holm (1979) method for multiple comparisons correction.

LFP spectrograms were computed using a Fourier transform with a Kaiser window with a frequency resolution of 0.15 Hz, temporal resolution of approximately 6 seconds, and with 50% overlapping windows. Spectrograms and their differences were smoothed in time with the resolution of half a minute, and in frequency with the resolution of 1Hz using median filter. To quantify the effect of CNO on LFP rhythms, we computed the spectrograms modulation index as follows. First, the channel-averaged spectrograms for the duration of the baseline recording was computed. Next, we averaged time-frequency spectral profiles over time, resulting in frequency-resolved spectral profiles. The effect of CNO was assessed by computing a modulation index, defined as the ratio of channel-averaged spectrogram after injection minus baseline, time-averaged spectrogram and the sum of the same quantities, for every time window and for every frequency. This modulation index ranges between -1 and 1, and describes the changes due to drug injection over time, for each frequency.

To obtain a statistical assessment of CNO effects across groups and bands, we computed the autocorrelation of spectrograms for every subject at every frequency, and resampled the spectrograms using only uncorrelated data bins based on the lag times identified. We next computed the median of the modulation index over different frequency bands defined as follows: Delta (1-4 Hz), Theta (4-8 Hz), Alpha (8-12 Hz), Beta (12-30 Hz), Low Gamma (30-70 Hz) and High Gamma (70-100 Hz). Data within each band were pooled over uncorrelated time points and over subjects, and the population medians were compared using two-sided Wilcoxon rank-sum tests, followed by Bonferroni-Holm correction.

Multielectrode coherence

To analyze multi-electrode recordings, channel averaged spectrograms were preprocessed as described above. (Temporal?) Smoothing was carried out using a one minute median filter as described above. As in our previous analyses, multielectrode recordings showed that the autocorrelation vanishes much sooner than one minute. We normalized post CNO spectrograms (30-40 post CNO injection window) with respect to the last 3 minutes of pre-CNO baseline using a modulation index as before.

Similar to the previous experiment, to obtain quantifiable assessment of the CNO effect across different groups and bands, data within each band were pooled over every one minute and subjects and the population medians were compared for each region separately using a two-sided Wilcoxon rank-sum tests, followed by Bonferroni-Holm correction.

For spectral power coherency, the magnitude of squared coherency was computed using Welch's overlapped averaged periodogram method (Welch, 1967) with a 50% overlapping window of 2 seconds length. The coherency was calculated on every one minute length of the channel averaged recordings. To see the effect of the drug, the magnitude squared coherency for the 30 minutes post injection time, was normalized to the time averaged coherency during last 3 minutes of the baseline at every time and frequency using a modulation index similar to spectrograms.

To assess the statistical significance between groups, the coherency modulation indices after 30 minutes of injection were pooled over every one minute (corresponding to uncorrelated data points) and the median over different frequency bands (same convention of bands as

before) were calculated for each region pair and compared using two-sided Wilcoxon rank-sum tests, followed by Bonferroni-Holm correction.

Furthermore, to see the effect of the CNO on the phase coupling between different areas as another assessment of signals becoming coherent, LFP data were first filtered using a third order Butterworth filter in delta band, and the instantaneous phase of each channel was computed by taking the phase of the analytical signal resulted from the Hilbert transform. Then, for all possible pair of channels belonging to two different regions, Phase Locking Value (PLV) was computed as follow:

$$\mathrm{PLV} = \frac{1}{\mathrm{N}}\left|\sum_{j=1}^{N} e^{i\left(\theta_{ch1}(t_j)-\theta_{ch2}(t_j)\right)}\right|$$

Where N is the number of data points in time and $\theta_{ch1}(t_j), \theta_{ch2}(t_j)$ are the instantaneous phase of the LFP of channel 1 and 2 at time j. This value would demonstrate the consistency of phase difference over time between LFP oscillations of different channels belonging to different regions. The PLV value for each pair during the 30 to 40 minutes post CNO was normalized to the PLV value of the last 3 minutes of the baseline using a modulation index and was pooled over channel pairs and animals. Finally, the population medians of the control and experimental group for each region pair were compared using two-sided Wilcoxon rank-sum tests, followed by Bonferroni-Holm correction.

3. Results

Chronic inhibition of the prefrontal cortex results in paradoxical fMRI over-connectivity

Structurally based models of rsfMRI connectivity posit that neural silencing of a network node would result in diminished functional coupling with regions anatomically linked to the affected substrate (Alstott et al., 2009; Grayson et al., 2016). To empirically test this hypothesis, we carried out rsfMRI measurements in a cohort of mice in which neuronal activity in the prefrontal cortex (PFC) was chronically inhibited via bilateral viral transduction of the inward rectifying potassium channel Kir2.1 under the control of a pan-neuronal promoter (**Fig. S 3.1A**). Prior research has shown that viral-mediated Kir2.1 expression results in a reduction of both evoked and spontaneous neuronal excitability lasting several weeks (Xue et al., 2014; Beier et al., 2017). In keeping with this, proof of concept *in vivo* electrophysiological recordings in the PFC of mice unilaterally transfected with Kir2.1 revealed a robust reduction of spontaneous firing rate in the targeted cortical area with respect to its control contralateral region (N=4, paired t-test, $p = 0.002$, **Fig. S3.3**).

We next compared the patterns of rsfMRI connectivity in Kir2.1 and GFP-transduced control littermates, by imaging Kir2.1 transfected mice four weeks after viral injections (**Fig. 3.1A**, **Fig. S3.1A**). Consistent with previous investigations (Bertero et al., 2018; Pagani et al., 2019), seed-based probing revealed significant long-range correlation between the PFC and thalamo-cortical components of the mouse default mode network in both cohorts (**Fig. 3.1B**). Surprisingly, between-group comparisons revealed foci of significantly *increased* rsfMRI connectivity in the posterior cingulate/retrosplenial cortex and centromedial thalamic regions of Kir2.1 transfected mice (*t*-test, $p < 0.05$, $t > 2.03$, FWE cluster-corrected, $p < 0.05$; **Fig. 3.1C**). Regional quantifications of DMN connectivity via multiple prefrontal-DMN seeds corroborated these findings, revealing increased rsfMRI synchronization along the entire

midline extension of this network (two-way ANOVA, $F_{(1, 33)} = 6.93$; p = 0.0128; **Fig. 3.1D**) and its centromedial thalamic targets (*t*-test, $t_{33} = 2.589$, p = 0.014; **Fig. 3.1E**). Voxel-wise mapping did not reveal any foci of reduced functional connectivity (t > 2.03, cluster correction at p < 0.05). Importantly, all the brain thalamo-cortical regions showing increased rsfMRI connectivity in Kir2.1 mice are characterized by high projections density from the PFC, as seen by comparing the magnitude of inter-group connectivity differences with incoming axonal connectivity strength inferred from a voxel-model of the mouse brain connectome (Coletta et al., 2020a) (Fig. **3.1F**, Wilcoxon rank sum test, p<0.0001). Together, these findings suggest that chronic inhibition of neural activity in the PFC results in paradoxically increased functional connectivity between long-range thalamo-cortical terminals of the mouse DMN.

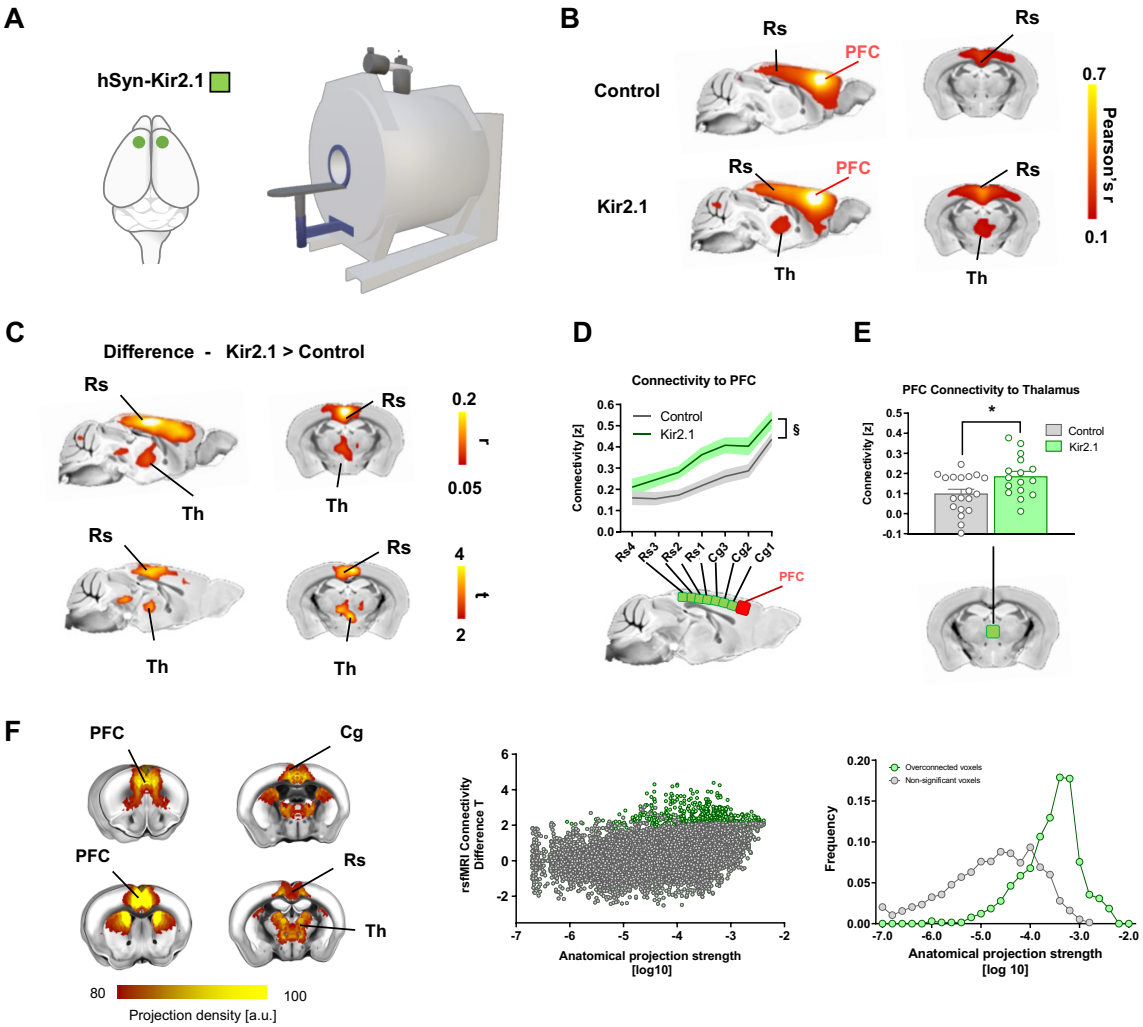

Figure 3.1 Chronic silencing of the PFC induces rsfMRI over-connectivity. (A) Summary of experimental design. The potassium channel Kir2.1 or GFP (control) were transduced bilaterally into the PFC of wild-type. Four weeks after viral injections, mice underwent rsfMRI scanning. (B) Seed based connectivity mapping of the PFC in GFP (control), and Kir2.1 transduced subjects. (C) Corresponding group difference maps. Area with significantly increased rsfMRI connectivity in Kir2.1 expressing mice are depicted in red-yellow (Pearson's r and T stat difference map). (D) Antero-posterior profiling of rsfMRI connectivity of the PFC within the midline axis of the mouse DMN. Note the increased connectivity throughout the antero-posterior extension of the mouse DMN in Kir2.1 expressing mice. (E) Fronto-thalamic rsfMRI overconnectivity in Kir2.1 expressing mice. (F) Regions exhibiting rsfMRI overconnectivity in Kir2.1 mice are robustly innervated by the PFC. Left: Axonal projections from the PFC (top 20% strongest connections). Middle: scatter plot illustrating intergroup differences in rsfMRI connectivity as a function of PFC structural connectivity strength. Green dots indicate functionally overconnected voxels. Right: Distribution of overconnected voxels as a function of axonal connectivity strength Green. DMN: Default Mode Network; Cg:

cingulate cortex; PFC: prefrontal cortex, RS: retrosplenial; Th: Thalamus. § $p<0.05$, 2-way ANOVA, repeated measurements; * $p<0.05$, student t test.

Chemogenetic inhibition of the prefrontal cortex leads to fMRI over-connectivity.

The observation of increased DMN connectivity upon chronic inhibition of PFC activity argues against a dyadic relationship between structural and functional connectivity. However, this finding could reflect complex neuroadaptive responses to chronic silencing. To corroborate the specificity of Kir2.1 findings and obtain mechanistic insight into the origin of the observed fMRI overconnectivity, we designed a new set of experiments in which DREADD-based chemogenetics was employed to induce a time-controlled, acute silencing of PCF activity during rsfMRI scanning. An overview of experimental procedures is provided in **Figure 3.2**. To enable remote silencing of fronto-cortical activity, we bilaterally transfected the PFC with the inhibitory hM4Di DREADD using a pan-neuronal human synapsin promoter (**Fig. 3.2A**). Three weeks after viral injection, control (GFP-transfected) and hM4Di-expressing animals underwent rsfMRI scanning or electrophysiological recordings before and after intravenous injection of the DREADD activator clozapine-N-oxide (CNO). To account for the slow pharmacokinetic profile of CNO in the rodent brain (Jendryka et al., 2019), both imaging and electrophysiological recordings were split into a pre-CNO injection baseline, a transitory (0 - 15 min) drug-equilibration period, and an active time window (15-50 min post CNO injection) to which all our analyses refer to, unless otherwise specified (**Fig. 3.2B-C**).

To assess whether acute chemogenetic silencing of the PFC results in rsfMRI oversynchronization, we compared rsfMRI connectivity patterns in hM4Di transfected and control mice upon acute CNO administration (active phase, **Fig. 3.3** and **Fig. S3.1B**). Recapitulating the Kir2.1 findings, voxel-wise mapping revealed foci of significantly increased rsfMRI connectivity in the posterior cingulate/retrosplenial cortices and midline thalamic

regions of DREADD-expressing mice (t-test, $P < 0.05$, FWE corrected, cluster defining threshold $t > 2.03$, $p < 0.05$; **Fig. 3.3A**). Regional quantifications corroborated the presence of rsfMRI oversynchronization along the cingulate and retrosplenial axis of the DMN, and between the PFC and medio-dorsal thalamic areas (2-way repeated measures ANOVA, $F_{1,32} = 6.58$; $p = 0.0155$; t test $t_{32} = 4.30$, $p = 0.001$, respectively; **Fig. 3.3B-C**), a set of regions characterized by dense incoming projections from the PFC (**Fig. S4**, Wilcoxon rank sum test, $p<0.0001$).

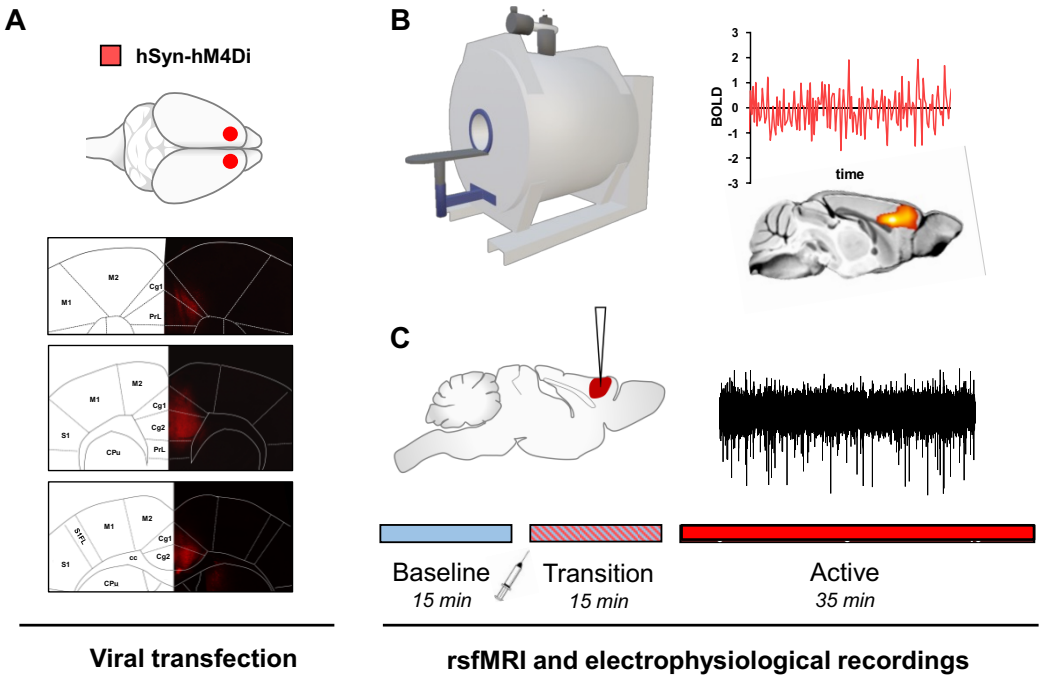

Figure 3.2 Experimental design of chemo-fMRI experiments. (A) AAV8-hSyn-hM4Di or AAV8-hSyn-GFP (control) were bilaterally injected into the PFC of wild type. The bottom panels show representative viral expression across three adjacent slices (viral injection in middle slice – see also Fig. S3.1B). Three weeks after transduction (B) mice underwent rsfMRI scanning or (C) electrophysiological recordings. A reference acquisition timeline is reported to depict timeseries binning into a 15 min pre-CNO reference baseline, a drug equilibration window (15 min, transition), and a 35 min CNO active time window (active).

Importantly, baseline PFC connectivity in these areas was comparable across groups (voxel-wise mapping, $Z>2.03$ cluster corrected, PFC-Cingulate, 2 way ANOVA, $F_{1,32} = 0.48$, $p = 0.49$, Thalamo-PFC, student t test, $t_{32} = 0.23$, $p = 0.81$), and oversynchronization gradually emerged

in the hM4Di cohort after CNO administration, peaking during the DREADD active time-window (t-test, $T_{32} = 2.158$, p = 0.03, PFC-Rs $T_{32} = 4.301$, p = 0.0001, PFC-Th, **Fig. 3.3D-E**). Moreover, no intergroup differences were observed in the characteristic hemodynamic response function in this area (kernel height p > 0.6; time-to-peak **p** > 0.12, full-width-at-half-peak **p** > 0.37,student *t*-test) nor were between-group differences in arterial blood pressure (p > 0.7, t test) or blood gas levels observed (P_aCO_2 p=0.49; P_aO_2 p =0.22, student t test). These control measurements rule out major spurious vascular or hemodynamic contributions and corroborating the specificity of the mapped changes. More broadly, our chemo-fMRI results show that acute inhibition of PFC activity results in a pattern of DMN oversynchronization closely recapitulating that observed with chronic Kir2.1-mediated silencing, suggesting that this phenomenon is not manipulation-specific, nor the indirect consequence of homeostatic reactivity to protracted neural silencing.

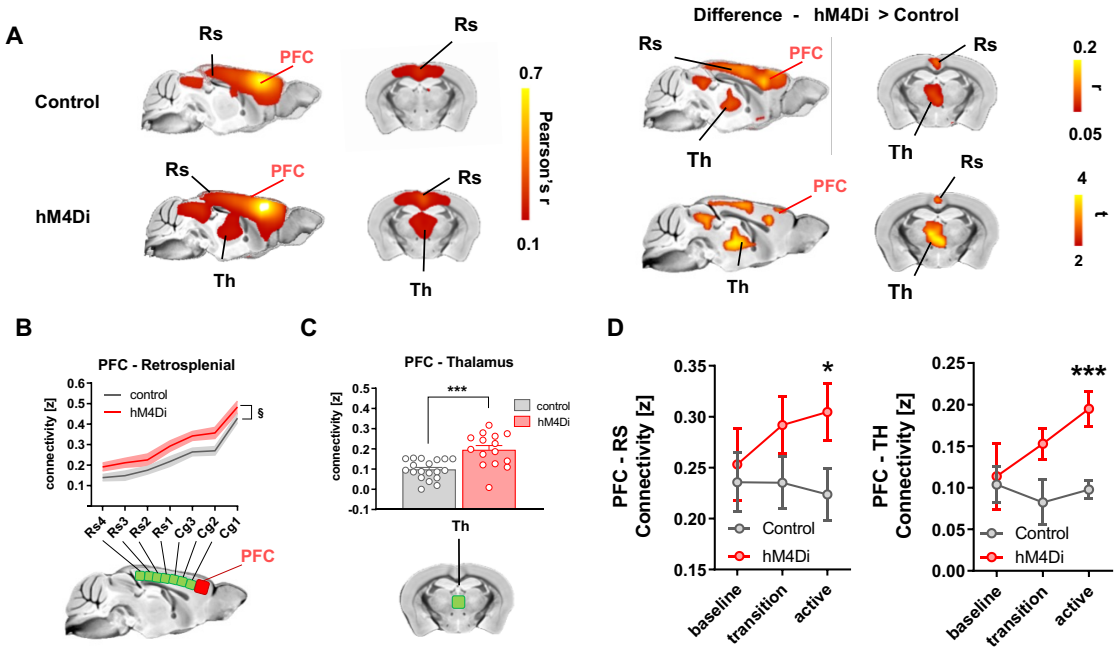

Figure 3.3 Chemogenetic silencing of the PFC results in DMN overconnectivity. (A) Seed-based connectivity of the PFC and between group difference map revealed rsfMRI over-connectivity in the DMN of hM4Di expressing

mice. (B) Antero-posterior profiling of rsfMRI connectivity of the PFC along the midline axis of the mouse DMN in the two cohorts. (C) Thalamo-cortical rsfMRI hyper synchronization in hM4Di expressing mice. (D) Prefrontal-retrosplenial and prefrontal-thalamic connectivity timecourse. Data are plotted as mean ± SEM. Cg: cingulate cortex; PFC: prefrontal cortex, RS: retrosplenial cortex; Th: Thalamus. § $p<0.05$, 2-way ANOVA repeated measurements, genotype; * $p<0.05$, *** $<p<0.001$, Student t test.

Chemogenetic silencing of the PFC increases interareal delta coherence

To probe the efficacy of chemogenetic silencing and investigate the neural correlates of the observed rsfMRI overconnectivity, we next carried out electrophysiological recordings in the PFC of hMD4i- or GFP-transduced control animals prior to and after CNO administration, under the same experimental conditions of rsfMRI (**Fig. 3.4**). Baseline electrophysiological traces revealed the presence of appreciable spontaneous multi-unit activity in the PFC both groups (mean firing rate 15.0 ± 2.2 spikes/s in hM4Di-expressing, and 14.1 ± 3.8 in GFP-transduced mice, n = 5 each group, p = 0.85, t test, **Fig. 3.4A-B**). As expected, CNO administration robustly inhibited firing rate in hM4Di expressing mice, but not in control GFP-transduced subjects (Fig. 4A-C, $p<0.01$, all timepoints, t test, followed by FDR correction). In keeping with the time-profile of rsfMRI overconnectivity, DREADD-induced PFC inhibition was characterized by gradual decrease of neural firing upon CNO administration, reaching a steady state approximately 15-20 min after the intravenous bolus (**Fig. 3.4C**).

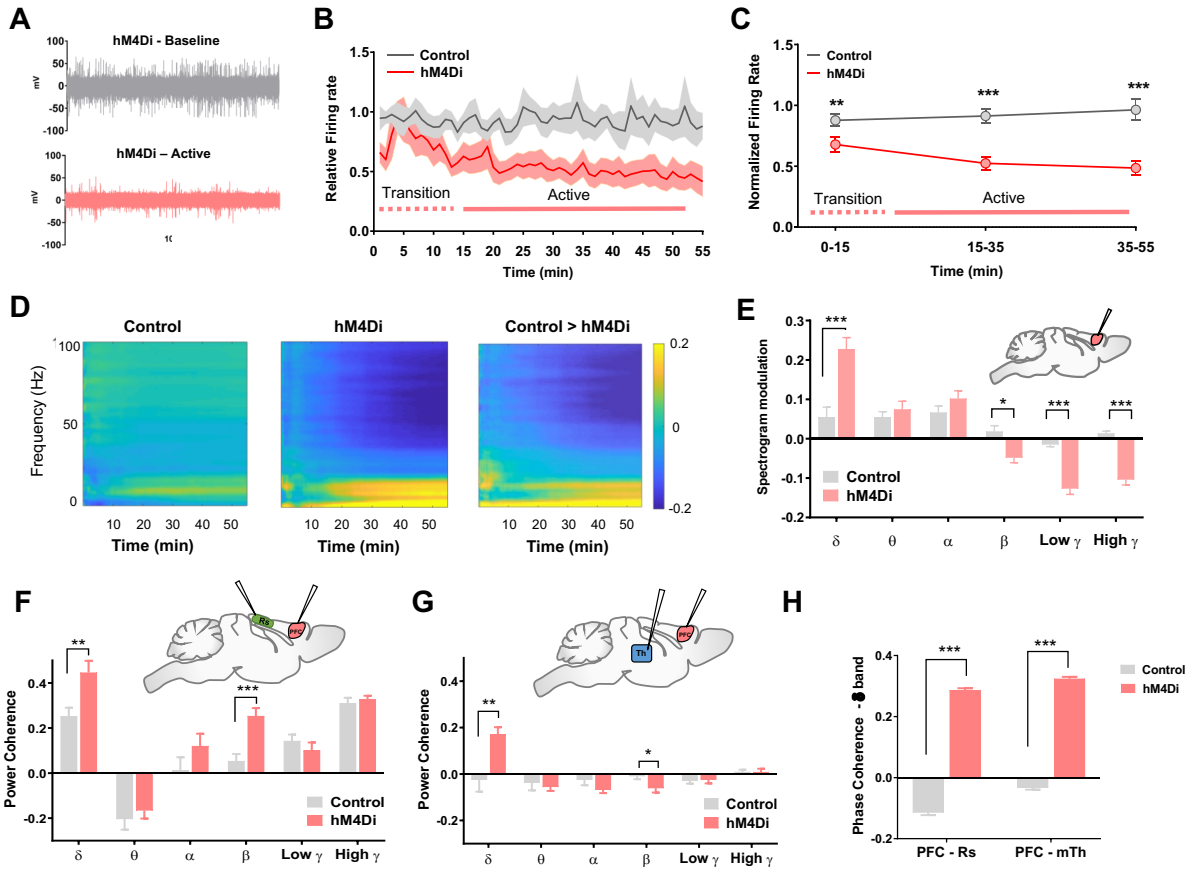

Figure 3.4 Chemogenetic silencing of the PFC results in increased delta activity. (A) Representative raw traces collected before and after CNO injection in a representative recordings site of hMD4i animal. (B-C) Reduced firing rate in hM4Di-expressing mice compared to GFP-transduced controls. (D) Mean post-injection spectrogram in control (Left), hM4Di-expressing animals (center), and mean between group difference (right). (E) Quantification of band-specific power spectrum changes upon CNO injection in both groups (F-G). Baseline normalized power coherence at different frequency bands for PFC-Thalamus (Left) and PFC-retrosplenial electrode pairs. (H). Baseline normalized phase coherence in delta band between PFC-retrosplenial and PFC-thalamus electrode pairs (mean ±SEM; *p <0.05, **p<0.01, ***p<0.001, Student T test, FDR corrected).

To obtain insight into the neural rhythms underlying the observed rsfMRI overconnectivity, we next analyzed local field potential (LFP) traces obtained from the same set of PFC electrophysiological recordings. Consistent with the observed firing rate reduction, LFP spectrograms from hM4Di-transduced animals, revealed a robust decrease in beta and gamma power after CNO administration with respect to CNO treated controls ($F_{1,22}$ = 239.4, p < 0.001, **Fig. 3.4D**). Notably, the power reduction in these frequency bands was also accompanied by a prominent increase in PFC delta power in DREADD-expressing subjects

(Fig. 4C-D, delta $p < 0.001$, theta $p = 0.77$; alpha $p = 0.34$; beta $p = 0.01$; low gamma $p<0.001$, high gamma $p<0.001$; Student t test, Bonferroni corrected).

Delta band fluctuations and slow oscillatory rhythms can effectively propagate across large cortical territories, hence promoting interaction and synchronization between distant brain areas (Massimini et al., 2004; Mitra et al., 2018). These properties led us to hypothesize that the observed overconnectivity could be primarily driven by increased interareal delta oscillatory coherence. To test this hypothesis, we carried out a set of simultaneous multi-electrode LFP recordings in the PFC, retrosplenial and centromedial thalamus of control and DREADD-transfected animals. These regions were selected to cover the anatomical substrates exhibiting the highest functional overconnectivity in our prior chemo-fMRI studies (cf. **Fig. 3.3**). Spectral-power quantifications after CNO administration revealed the presence of a robust reduction in gamma power in all the three recording sites, together with an increased delta activity in the PFC, but not in retrosplenial or centromedial thalamus of DREADD-transfected animals (**Fig. S3.5**). Notably, power coherence measurements revealed the presence of robustly increased delta coherence between PFC–retrosplenial and PFC-thalamus, recapitulating imaging findings of increased functional synchronization between these areas (**Fig. 3.4F-G**). Increase and decreased beta band coherence were also observed between PFC-Thalamus and PFC– restrosplenial, respectively, while no other between-group change in coherence was observed at all the other examined bands (**Fig. 3.4F-G**). Importantly, the observed increased in delta power coherence between PFC–Thalamus and PFC–retrosplenial was paralleled by a similarly robust increase in delta *phase* coherence between these electrode pairs in DREADD expressing animals (**Fig. 3.4H**). Taken together, these results support a neural origin for the our imaging findings, and implicate increased inter-areal coherence in delta oscillatory bands as a plausible driver of the observed rsfMRI over-synchonrization.

The polymodal thalamus relays oversynchronization to wider cortical areas

Although delta oscillations can originate both at the cortical and thalamic level (Sanchez-Vives and McCormick, 2000), it has now been conclusively demonstrated that the full expression of slow rhythms requires active thalamic participation (Hughes et al., 2002; David et al., 2013). Of potential mechanistic relevance, our chemo-fMRI study revealed a prominent oversynchronization of the PFC with centro-medial areas of the thalamus, a set of higher-order polymodal nuclei that have been recently shown to play a causal role in the generation of delta oscillations, and their propagation to large neocortical territories (Gent et al., 2018; Adamantidis et al., 2019). According to these recent investigations, reduced asynchronous cortical input from the silenced PFC may lead to the emergence of enhanced cortico-cortical and cortico-thalamic slow-oscillatory activity, an effect that could in turn be relayed back to wider cortical regions by polymodal thalamic areas. Within such a framework, the thalamo-prefrontal profiles of rsfMRI overconnectivity observed after chemogenetically inhibiting the PFC should thus be spatially segregable into centro-medial (polymodal) and lateral (unimodal) components, the former being oversynchronized with wider cortical territories. To explore this hypothesis, we clustered voxels in the thalamus based on unique between-group functional connectivity differences (Schleifer et al., 2017). This approach led to the identification of two main thalamic sub-territories, one corresponding to the centro-medial (polythalamic) portion of this area, and the second encompassing latero-thalamic (sensory) areas (**Fig. 3.5A**). Notably, seed-based probing of the unimodal thalamus did not reveal significant differences between hM4Di-expressing and control animals ($Z > 2.03$, all voxels, cluster corrected with cluster defining threshold of $t > 2.03$). By contrast, seed-based probing of the polymodal thalamus in hM4Di expressing mice revealed a widespread pattern of cortical overconnectivity exceeding the boundaries of the PFC to encompass motor and somatosensory territories, including the retrosplenial cortex (**Fig. 3.5B-C**; $Z > 2.03$, cluster corrected, $p < 0.05$, **Fig. 3.5C**,

p <0.04 all regions, t test, FDR corrected, ROI location in Fig. **S3.7**). The observation of increased rsfMRI coupling between the centromedial thalamic and the retrosplenial cortex (Fig. 5C) prompted us to examine neural coherence between these two locations from previous multi-electrode recordings. In keeping with imaging findings, we found a robust increase in delta power coherency between these two locations (**Fig. S3.5A**), an effect associated with augmented coherence also in the beta and gamma bands. Interestingly, Thalamo-retrosplenial LFP recordings also exhibited significantly increased delta phase coherence in DREADD-expressing animals with respect to control subjects (**Fig. S3.5B**). Overall, these findings support a model in which cortical silencing, and the consequent reduction in high frequency asynchronous output (**Fig. 3.5F**) may lead to enhanced delta coherence, a result of reduced cross-frequency interactions between the silenced area and its cortico-cortical and cortico-thalamic targets. This effect may in turn be gated and propagated by polymodal thalamic to produce wider cortical over-synchronization (**Fig. 3.5G**).

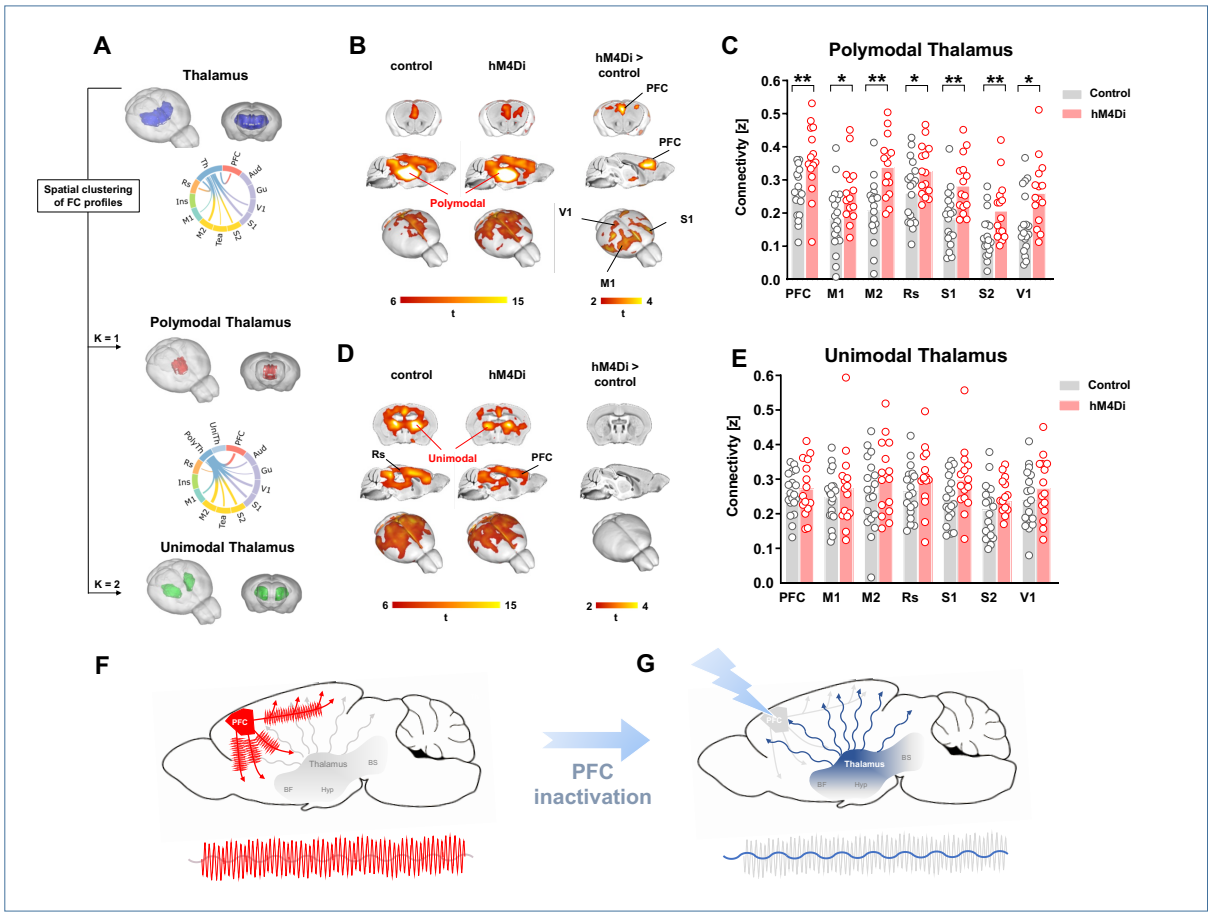

Figure 3.5 The polymodal thalamus relays rsfMRI oversynchronization to cortical areas. (A) k-means clustering of PFC-thalamic rsfMRI connectivity profiles (thalamus, blue, unimodal thalamus, green; polymodal thalamus, red) and circular representation of between-group connectivity difference of the entire thalamus and thalamic partition (UniTh: unimodal; PolyTh: polymodal thalamus). (B-D) Seed connectivity of sub-thalamic partitions, between group difference maps (B,C polymodal thalamus; D-E, unimodal thalamus) and corresponding quantification of thalamo-cortical connectivity (*p<0.05, **p<0.01; Benjamini-Hochberg corrected). (F) A possible interpretative model of our findings. Under basal conditions the PFC sends asynchronous output to cortical and centromedial thalamic regions (red waves). Cortical inactivation (G) reduces high frequency input to cortical and centro-medial thalamic areas, reducing cross-frequency neural interactions. This in turns results in an enhanced global slow oscillatory activity (blue wave) and rsfMRI coupling, an effects that is likely to contain cortico-thlamic as well as remotely generated slow oscillatory input (i.e. neuromodulatory input from basal forebrain – BF, brainstem – BS and hypothalamus - Hyp). Locally- or remotely generated delta activity can then be gated and further propagated by centro-medial thalamic nuclei to wider cortical areas as in Gent et al., 2019.

3. 4. Discussion

Here we used viral and chemogenetic manipulations to causally deconstruct brain-wide measurements of interareal functional connectivity based on rsfMRI. In contrast to prevailing structurally-driven interpretations of rsfMRI connectivity, we found that chronic and acute neural silencing of the mouse PFC results in paradoxically increased rsfMRI connectivity. Further investigations using in vivo electrophysiology revealed that PFC silencing is associated with prominently increased delta coherence, arguing against a spurious vascular origin for the observed hyper-connectivity, and implicating a key contribution of locally- and remotely-generated slow oscillatory rhythms to the establishment of brain-wide rsfMRI coupling. Together, the results of our causal perturbations suggest that rsfMRI-based measures of functional connectivity do not monotonically reflect interareal axonal connectivity, and highlight a critical contribution of subcortical rhythm generators to the establishment of brain-wide functional coupling.

The observation that structural and functional connectivity strength are correlated both at the whole-brain and mesoscopic scale (Hagmann et al., 2008; Wang et al., 2013; Coletta et al., 2020a) lies at the basis of structurally-based models of rsfMRI connectivity, according to which spatiotemporal correlations in spontaneous rsfMRI activity are critically shaped and constrained by underlying axonal connectivity (Friston and Büchel, 2006; Alstott et al., 2009; Grayson et al., 2016). An often implicit assumption of these models is that regional inactivation of a neural node would result in disrupted functional synchronization in distributed target areas, the spatial extent of which is dictated by the structural topography of the affected region (Alstott et al., 2009). A chemo-fMRI study in primates has provided initial empirical evidence in support of this interpretative framework, by showing that hM4Di-mediated silencing of the amygdala produced disrupted rsfMRI coupling with cortical areas anatomically linked to this region.

Leveraging the recent implementations of chemo-fMRI in the mouse (Giorgi et al., 2017) here we expanded these investigations to probe how cortical silencing affects brain-wide rsfMRI coupling. Motivated by reports describing paradoxical hyperconnectivity in clinical conditions characterized by physical disruption of neural nodes (Hillary and Grafman, 2017), we first carried out proof-of-principle experiments using chronic silencing of neural activity in the mouse PFC via overexpression of a potassium channel. We next ran a set of mechanistic investigations leveraging acute chemogenetic inactivation of prefrontal activity via DREADDs. Surprisingly, we found that both chronic and acute silencing of the PFC paradoxically increased rsfMRI connectivity within thalamo-cortical substrates of the mouse DMN, encompassing cortical and subcortical regions densely innervated by prefrontal areas.

Our results advance our understanding of the principles underlying brain-wide rsfMRI coupling in two main directions. First, the observed breakdown between cortical output and rsfMRI coupling challenges prevailing structurally based interpretations of functional connectivity, suggesting that rsfMRI-based measures of functional coupling do not monotonically reflect reciprocal axonal output under all brain states and conditions, but can be critically influenced by remotely generated oscillatory rhythms, overriding direct interareal interactions. It should be emphasized here that this result should not be intended as a refutation of the strong structural basis of rsfMRI connectivity, but rather the basis of an updated model in which large-scale cortical coupling is strongly biased by synchronized input from global rhythm generators. Second, our results also provide a novel reference framework for the interpretation and reverse engineering of rsfMRI overconnectivity observed in brain pathology, especially in degenerative states characterized by paradoxical functional hypersynchronization. Although compounded by pathophysiological rearrangements in synaptic activity (Busche and Konnerth, 2016), observations of functional overconnectivity in neurological conditions

characterized by loss of cortical tissue (such as Alzheimer's disease) have been conceptualized as the result of compensatory rerouting of signal propagation along indirect structural paths, a neuroadaptive strategy aimed at maintaining task performance (Hillary and Grafman, 2017; Pusil et al., 2019). Our findings offer an alternative network-level mechanism for these clinical observations, suggesting that rsfMRI overconnectivity may reflect macroscale imbalances in cortico-thalamic input and increased slow oscillatory activity, a conceivable scenario in early-stage degenerative or neurological states characterized by loss of neuronal function in higher order cortical areas. MEG and EEG studies in neurodegenerative brain disorders provide indirect support to this hypothesis, as evidence of robust delta hyper-synchronicity in Alzheimer's disease patients has been repeatedly reported, an effect that appears to preferentially involve polymodal cortical areas (Huth et al., 2012; Ranasinghe et al., 2020). Within such a framework, functional impairments in cortical activity following degenerative pathology could manifest as hyper-synchronization during predisease states, eventually reverting to hypotrophy-associated under-connectivity at advanced stages of brain pathology.

Whilst a neural mass phenomenon like interareal rsfMRI coupling cannot be mechanistically dissected into discrete circuital elements, converging findings in our work support the involvement of higher-order thalamic regions and other remote global rhythm generators to the establishments of brain-wide rsfMRI coupling. These include the key involvement of increased delta coherence as a plausible neural driver of the mapped overconnectivity, the presence of foci of hyperconnectivity in higher order thalamic areas as well as the observation of increased functional coupling between polymodal thalamic nuclei and wider cortical territories in our chemo-fMRI manipulations. While rsfMRI synchronization may encompass nested multi-band contributions (Mantini et al., 2007; Siegel et al., 2012), delta oscillations are

optimally suited to promote interactions and synchronization between distant brain areas owing to their ability to effectively propagate across large cortical territories (Massimini et al., 2004; Mitra et al., 2018). In keeping with this, prior reports have linked rsfMRI connectivity to slow oscillatory activity (including delta rhythms), an association that appears to be especially prominent in states of low arousal, sleep or under light sedation (Lu et al., 2007; Wang et al., 2012; Lu et al., 2014; Neuner et al., 2014; Chan et al., 2017). Our electrophysiological recordings expand these findings suggesting that enhanced delta rhythm coherence serves as key effectors of oversynchronization produced by reduced cortico-cortical and cortico-thalamic input.

Although both cortical and thalamic regions may contribute to the increased delta coherence mapped in our chemo-fMRI study (Sanchez-Vives and McCormick, 2000; Hughes et al., 2002), full expression of delta rhythms is thought to require active thalamic participation (Hughes et al., 2002; David et al., 2013). Recent circuital dissections have revealed a critical role of higher-order thalamic nuclei in generating and propagating delta rhythms to the PFC and other cortical areas (Gent et al., 2018). This observations support a model in which enhanced delta activity could be relayed by polymodal thalamic nuclei sfMRI hyper-synchronization across large cortical regions. It should however be noted that other neural mechanisms or regional substrates (such as the claustrum, Narikiyo et al., 2020) could contribute to the observed oversynchronization, including the back-propagation of cortically (PFC) generated delta activity (Massimini et al., 2004), or a role for nested or adjacent frequency bands (e.g. infra-slow activity (Mateo et al., 2017; Mitra et al., 2018)). Similarly, ascending neuromodulatory systems are likely to exert a key contribution in the generation of delta oscillatory activity and the global interregional coupling underlying canonical rsfMRI connectivity and aberrant rsfMRI coupling (Safaai et al., 2015; Reimann and Niendorf, 2020).

Importantly, because sedation shifts relative LFP power from higher-frequency neural activity to slow rhythms (Franks, 2008), the direction and distribution of the connectivity changes we mapped, and their neurophysiological signatures, are likely to be brain-state dependent and could differ under awake or high arousal conditions. Such a scenario does not however diminish the relevance of our findings for two main reasons. First, the observation of increased rsfMRI coupling in the face of robust neural silencing in the PFC is sufficient to disprove a monotonic relationship between interareal coupling and rsfMRI connectivity, and serves as a demonstration for a non-dyadic relationship between these two entities, with implications both for the mechanistic modelling of rsfMRI coupling and for the back engineering of rsfMRI signals recorded in brain disorders. Second, it should be noted that the light sedation regimen employed in this study is physiologically stable (cf. Fig B,D), preserves sensorial responsivity (Orth et al., 2006) and does not induce burst-suppression or cortical hyper-synchronization (Liu et al., 2011), resulting in preserved rsfMRI connectivity topography (Coletta et al., 2020b; Whitesell et al., 2020) and state dynamics (Gutierrez-Barragan et al., 2018). These properties make the brain state under which our recordings were carried out not dissimilar from the quiet wakefulness conditions, often bordering into sleep, (Tagliazucchi and van Someren, 2017)) that characterize most rsfMRI scanning in humans (Reimann and Niendorf, 2020). In keeping with this notion, recent intracranial recordings under conditions of quiet wakefulness have revealed the presence of significant epochs of delta activity in rodents (Crochet and Petersen, 2006; Vyazovskiy et al., 2011), primates (Lakatos et al., 2008) as well as humans (Sachdev et al., 2015). Because of the difficulty in controlling restraint-induced stress in highly rousable rodent species (Wang et al., 2017; Reimann and Niendorf, 2020), the state-dependence of our manipulation is an interesting subject for future investigations which can benefit from the implementation of hemodynamic mapping in quite wakefulness, for example using functional ultrasound imaging (Osmanski et al., 2014).

The stark contrast between our findings and the results of Grayson and associates (Grayson et al., 2016) calls for a critical discussion of possible experimental factors underscoring such divergent findings. One possible explanation could be related to the specific wiring diagram of the regions silenced in the two studies, as the PFC and the amygdala are characterized by very different connectivity profiles, are ontologically segregable, and exhibit different interaction patterns with subcortical rhythm generators. Discrepant experimental designs, including the lack of explicit control for the effects of CNO per se, and the use of a different contrast mechanism (cerebral blood volume vs. BOLD) in Greyson et al. could also partly explain these differences. Importantly, both the present study and the work from Grayson et al., were carried out under a very similar light sedation regimen, arguing against a prominent contribution of state-dependent differences in the sign and distribution of the observed rsfMRI changes.

In summary, our results document that cortical silencing results in paradoxical rsfMRI brain-wide overconnectivity and delta over-synchronization, pointing at a critical contribution of subcortical rhythm generators to the establishment of brain-wide functional coupling. Tour work also provide a testable network-level mechanism for reverse engineering of rsfMRI overconnectivity, suggesting that aberrant rsfMRI coupling can reflect macroscale imbalances in higher-order cortico-thalamic activity. The observed breakdown between cortical output and rsfMRI coupling promotes an updated view in which functional connectivity is critically orchestrated by the contribution of locally and remotely generated slow-oscillatory rhythms.

3. 5. Supplementary material

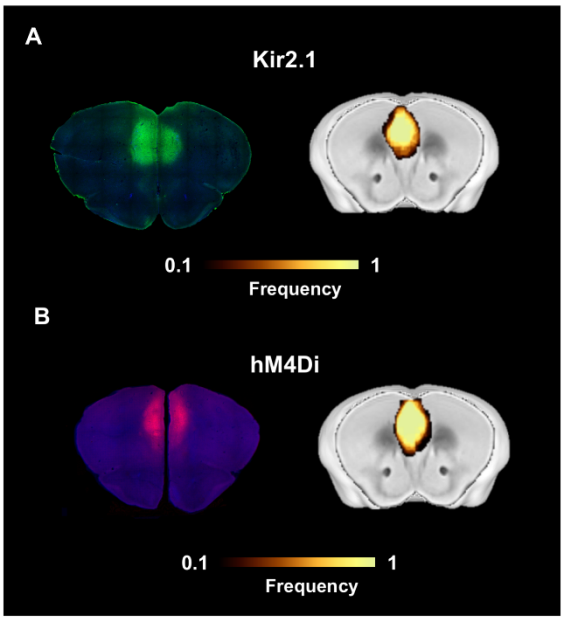

Figure S3.1 Viral expression localization. Brain sections showing (A) Kir2.1 and (B) hM4Di (red) expression. Heat maps illustrate regional quantifications of viral expression across subjects.

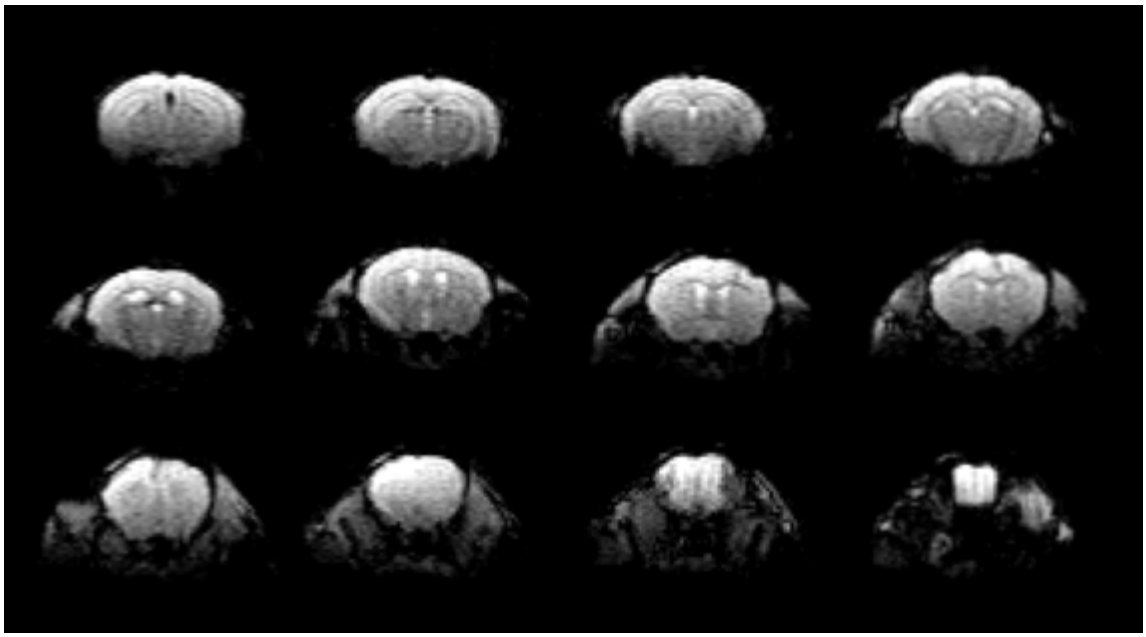

Figure S3.2 Raw data of a DREADDs-expressing mouse. A representative figure.

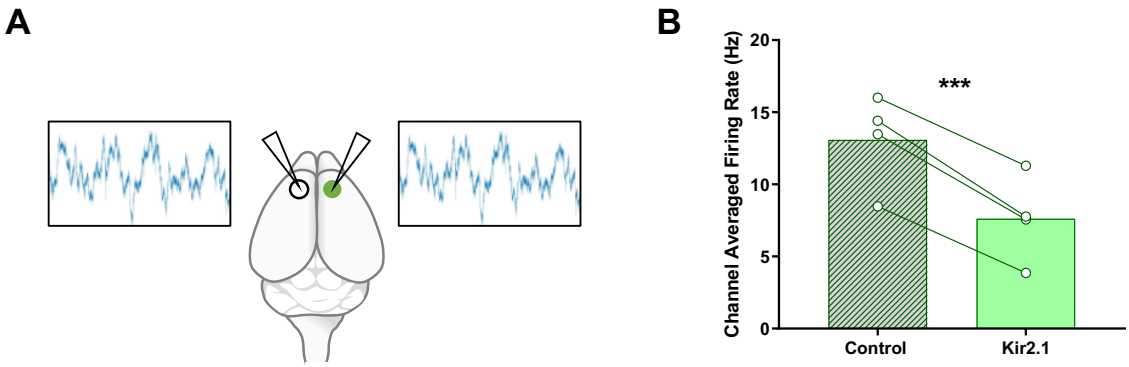

Figure S3.3 Over-expression of the potassium channel Kir2.1 in the PFC reduces spontaneous neural activity.Overexpression of the potassium channel Kir2.1 in the PFC reduces spontaneous neural activity. (A) Experimental design: Kir2.1 injection was performed unilaterally in the right PFC. A viral vector encoding GFP was injected in the contralateral area. Electrophysiological recordings were carried out bilaterally using a four shank

electrode. (B) Channel average firing rate for the control side (no Kir2.1 expression), and side expressing Kir2.1. (n=4; ** p<0.005).

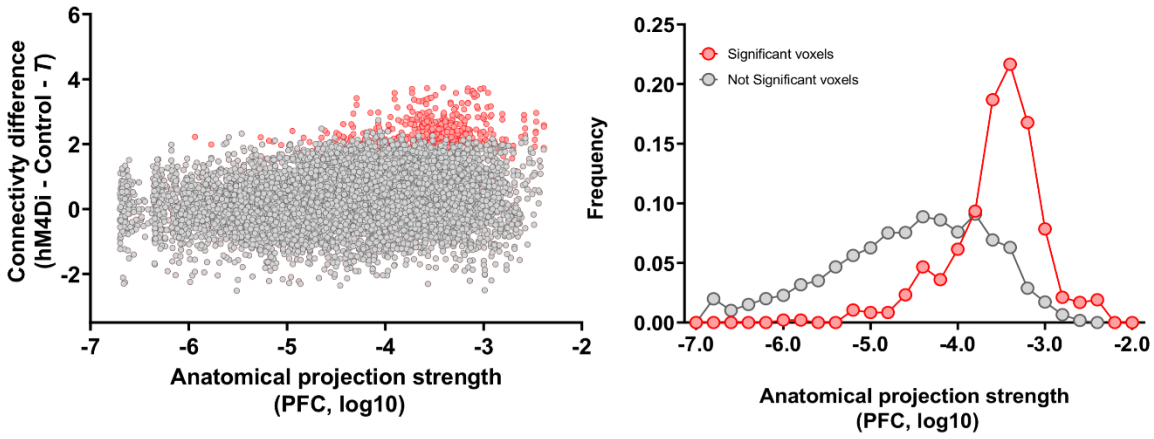

Figure S3.3 Regions exhibiting rsfMRI overconnectivity upon chemogenetic silencing of the PFC are robustly innervated by the PFC. Scatter plot illustrating intergroup differences in rsfMRI connectivity as a function of PFC structural connectivity strength. Note that all significantly hyperconnected voxels contain robust projections from the PFC. Red: voxels exhibiting the most significant rsfMRI connectivity (T>2.04, cluster corrected). Grey: non significant voxels.

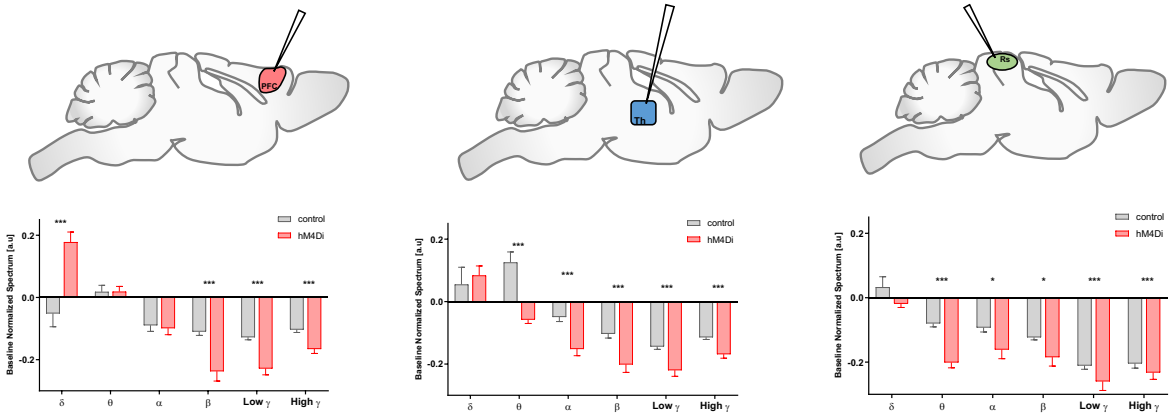

Figure S3.4 Quantification of band-specific power spectrum changes upon CNO injection in the PFC (left), centromedial thalamus (center) and retrosplenial cortex (right). Power was quantified with respect to pre-injection baseline (mean ±SEM; *p <0.05, **p<0.01, ***p<0.001, Student T test, FDR corrected).

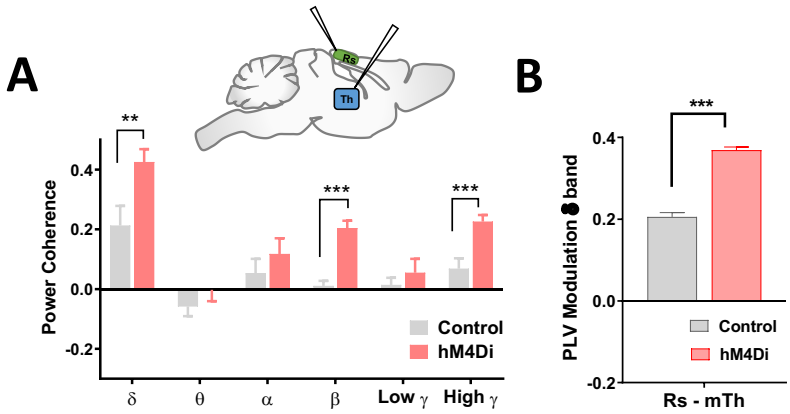

Figure S3.6 Multielectrode coherence between retrosplenial cortex and thalamus. (A) Baseline normalized power coherence at different frequency bands for Rs-Thalamus electrode pair (B) Baseline normalized phase coherence in delta band between Rs-thalamus electrode pair (mean ±SEM; *p <0.05, **p<0.01, ***p<0.001, Student T test, FDR corrected).

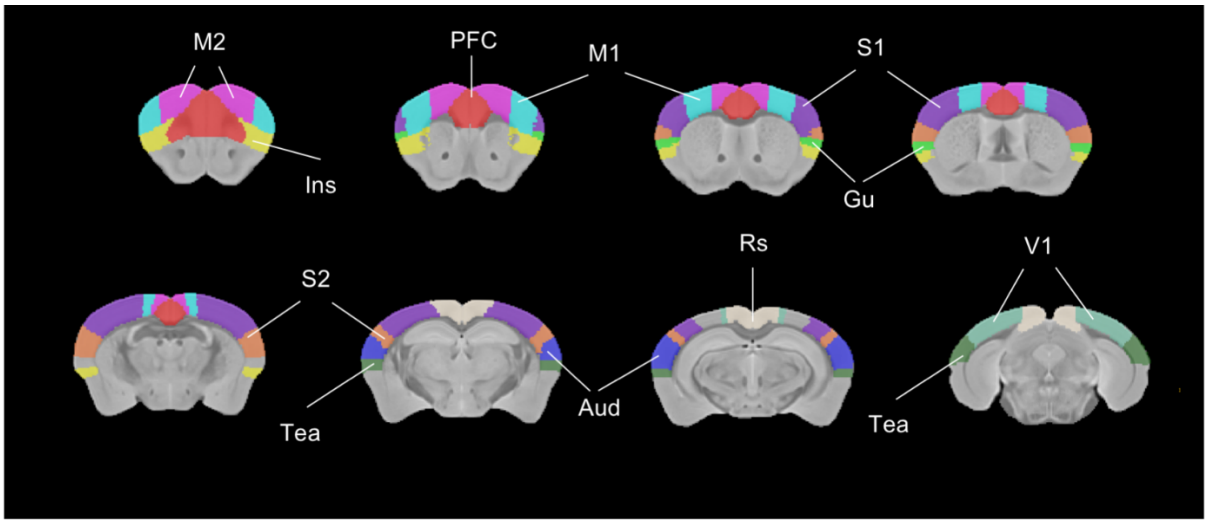

Figure S3.7 Anatomical location of volumes of interest employed for regional quantification of cortico-thalamic connectivity. Aud: auditory cortex; Gu: gustatory cortex; Ins: Insula; M1: primary motor cortex; M2: secondary motor cortex; PFC: prefrontal cortex, RS: retrosplenial; S1: primary somatosensory cortex; S2: secondary somatosensory cortex Tea: Temporal associate cortex; V1: visual area.

4. Future Perspectives

Nowadays, different silencing strategies for neuronal activity are available (Wiegert *et al*, 2017). In the present study, we decided to induce the expression of modified proteins using genetically encoded tools in order to achieve spatial and cellular specificity (Cho, 2015). Moreover, in the lab, we have generated evidence that chemo-fMRI is optimally suited to causally probe the brain-wide response to neuronal manipulation (Giorgi *et al*, 2017). One potential drawback of this strategy is however its inability to completely shut-down neuronal firing in vivo, resulting instead in a robust, yet incomplete, inhibition of neuronal firing, owing to the residual activity of afferent incoming axons. While this aspect can limit some of the inferences made with this tool, it should be noted that the reduced firing obtained appears to be properly suited to model the effect of disease related imbalances in neuronal activity, in which total loos of function is very rarely happening.

Local infusion of drugs such as the sodium channel blocker tetrodotoxin (TTX) could have been alternatively used in our study, leading to complete abolition of neuronal activity (Vinokurova *et al*, 2018). While a large body of literature demonstrates the efficacy of those tools, TTX has been used mainly for *in vitro* studies, and its administration in vivo is technically cumbersome, in the confined space of a MRI-magnet bore, and requires chronic cannula insertion, potentially causing neuronal death or lesion and complicating neural recordings. For these reasons we opted for the use of chemogenetic tools. Future comparisons of chemogenetically and TTX-evoked silencing are warranted to further corroborate the validity of our findings.

The combination of advanced methods for manipulating brain activity in the rodent brain with rsfMRI provides a powerful platform that promises to advance our understanding of the neural basis of brain-wide functional coupling in health and disease. Linking neural circuit activation at the whole-brain level to neuronal activity at cellular level remains one of the major challenges in current systems neuroscience. In this respect, the emerging evidence of consistent large-scale network mapping across laboratories is highly promising, and shapes a bright future for rsfMRI connectivity mapping in rodents as a means to crucially bridge the explanatory gap between cellular/microscale neurophenomena and large-scale neural dynamics in health and pathology across investigational scales. Within this framework, chemo-fMRI (Giorgi et al., 2017) appears to be optimally suited for a precise deconstruction and manipulation of steady-state network activity, enabling the identification of the fundamental elements that are necessary and sufficient to the establishment of brain-wide coupling.

The results reported in this thesis represent a clear example of the transformational power of this approach, highlighting a set of novel and somewhat unexpected findings that challenge current interpretation of functional connectivity. An interesting and highly warranted extension of the research platform here is its use to reverse engineer functional dysconnectivity in brain disorders. While initially designed to recapitulate prefrontal functional hypoconnectivity observed across mouse models of autism (Bertero et al., 2018; Liska et al., 2018), our manipulations revealed that prefrontal silencing results instead in hypersynchronization, suggesting that the phenotype observed in the mouse is the possible result of an opposing effect, i.e. the presence of overexcitability in the same regions, leading to network desynchronization, a notion consistent with evidence of dysfunction in pyramidal excitatory (CamKII positive) and GABAergic inhibitory neuronal populations associated with severe developmental disorders (Gonzalez-Burgos et al., 2015; Zikopoulos and Barbas, 2013). Such

an effect can also be linked to compelling investigations linking altered excitatory inhibitory (E/I) imbalance to social impairments in the mouse using optogenetics (Yizhar et al., 2011b). Our platform can be expanded to causally probe this relationship by using chemogenetically induced E/I increase for instance by exciting prefrontal pyramidal neurons and by inhibiting interneurons (GABA). Preliminary experiments in the lab aimed to probe this hypothesys demonstrate that increasing local E/I imbalances does indeed results in the predicted reduced functional connectivity (as well as social impairments in the mouse), confirming the predictive value of our framework. The extension of these investigation to other brain regions, and a full unravelling of the dependence of these findings with respect to brain state (i.e. anesthesia, and awake conditions) are expected to greatly advance our understanding of the origin and significance of rsfMRI aberrancies observed in ASD and related neuropsychiatric disorders.

5. References

Armbruster, B.N., Li, X., Pausch, M.H., Herlitze, S., Roth, B.L., 2007. Evolving the lock to fit the key to create a family of G protein-coupled receptors potently activated by an inert ligand. Proc. Natl. Acad. Sci. U. S. A. 104, 5163–8.

Arthur, D., Vassilvitskii, S., 2007. K-means++: The advantages of careful seeding. Proc. Annu. ACM-SIAM Symp. Discret. Algorithms 07–09–Janu, 1027–1035.

Beckmann, C.F., DeLuca, M., Devlin, J.T., Smith, S.M., 2005. Investigations into resting-state connectivity using independent component analysis. Philos. Trans. R. Soc. B Biol. Sci. 360, 1001–1013.

Bender, D., Holschbach, M., Stöcklin, G., 1994. Synthesis of n.c.a. carbon-11 labelled clozapine and its major metabolite clozapine-N-oxide and comparison of their biodistribution in mice. Nucl. Med. Biol. 21, 921–925.

Bertero, A., Liska, A., Pagani, M., Parolisi, R., Masferrer, M.E., Gritti, M., Pedrazzoli, M., Galbusera, A., Sarica, A., Cerasa, A., Buffelli, ario, Tonini, R., Buffo, A., Gross, C., Pasqualetti, M., Gozzi, A., 2018. Autism-associated 16p11.2 microdeletion impairs prefrontal functional connectivity in mouse and human. Brain 141, 2055–2065.

Bifone, A., Gozzi, A., Schwarz, A.J., 2010. Functional connectivity in the rat brain: a complex network approach. Magn. Reson. Imaging 28, 1200–1209.

Biswal, B., Zerrin Yetkin, F., Haughton, V.M., Hyde, J.S., 1995. Functional connectivity in the motor cortex of resting human brain using echo-planar mri. Magn. Reson. Med. 34, 537–541.

Boyden, E.S., Zhang, F., Bamberg, E., Nagel, G., Deisseroth, K., 2005. Millisecond-timescale, genetically targeted optical control of neural activity. Nat. Neurosci. 8,

1263.

Buckner, R.L., Andrews-Hanna, J.R., Schacter, D.L., 2008. The brain's default network: Anatomy, function, and relevance to disease. Ann. N. Y. Acad. Sci. 1124, 1–38.

Bullmore, E.T., Sporns, O., Solla, S.A., 2009. Complex brain networks: graph theoretical analysis of structural and functional systems. Nat. Rev. Neurosci. 10, 186–98.

Cavanna, A.E., Trimble, M.R., 2006. The precuneus: A review of its functional anatomy and behavioural correlates. Brain 129, 564–583.

Chai, X.J., Castan, A.N., Unger, T., Whitfield-Gabrieli, S., 2012. Anticorrelations in resting state networks without global signal regression. Neuroimage 59, 1420–1428.

Chow, B.Y., Han, X., Dobry, A.S., Qian, X., Chuong, A.S., Li, M., Henninger, M.A., Belfort, G.M., Lin, Y., Monahan, P.E., 2010. High-performance genetically targetable optical neural silencing by light-driven proton pumps. Nature 463, 98.

Clinton, S.M., Meador-Woodruff, J.H., 2004. Thalamic dysfunction in schizophrenia: neurochemical, neuropathological, and in vivo imaging abnormalities. Schizophr. Res. 69, 237–253.

Cole, M.W., Pathak, S., Schneider, W., 2010. Identifying the brain's most globally connected regions. Neuroimage 49, 3132–3148.

Crick, F., 1999. The impact of molecular biology on neuroscience. Philos. Trans. R. Soc. London B Biol. Sci. 354, 2021–2025.

Crick, F.H.C., 1979. Thinking about the Brain. Sci. Am. 241, 219–233.

Damoiseaux, J.S., Rombouts, S.A.R.B., Barkhof, F., Scheltens, P., Stam, C.J., Smith, S.M., Beckmann, C.F., 2006. Consistent resting-state networks across healthy subjects. Proc. Natl. Acad. Sci. U. S. A. 103, 13848–13853.

de la Torre-Ubieta, L., Won, H., Stein, J.L., Geschwind, D.H., 2016. Advancing the understanding of autism disease mechanisms through genetics. Nat. Med. 22, 345.

Durdon, K.G., 2008. Autism Risk Factors: genes, environmental, and gene-environmental interactions. Occup. Med. Oxford Engl. 21, 198–207.

Farrell, M.S., Roth, B.L., 2013. Pharmacosynthetics: Reimagining the pharmacogenetic approach. Brain Res. 1511, 6–20.

Ferrari, L., Turrini, G., Crestan, V., Bertani, S., Cristofori, P., Bifone, A., Gozzi, A., 2012. A robust experimental protocol for pharmacological fMRI in rats and mice. J. Neurosci. Methods 204, 9–18.

Fox, M.D., Raichle, M.E., 2007. Spontaneous fluctuations in brain activity observed with functional magnetic resonance imaging. Nat. Rev. Neurosci. 8, 700–711.

Fox, M.D., Snyder, A.Z., Vincent, J.L., Corbetta, M., Van Essen, D.C., Raichle, M.E., 2005. The human brain is intrinsically organized into dynamic, anticorrelated functional networks. Proc. Natl. Acad. Sci. U. S. A. 102, 9673–9678.

Friston, K.J., 2011. Functional and effective connectivity: a review. Brain Connect. 1, 13–36.

Friston, K.J., Frith, C.D., 1995. Schizophrenia: a disconnection syndrome. Clin Neurosci 3, 89–97.

Gabrielsen, T.P., Anderson, J.S., Stephenson, K.G., Beck, J., King, J.B., Kellems, R., Top, D.N., Russell, N.C.C., Anderberg, E., Lundwall, R.A., Hansen, B., South, M., 2018. Functional MRI connectivity of children with autism and low verbal and cognitive performance. Mol. Autism 9, 67.

Galvan, A., Caiola, M.J., Albaugh, D.L., 2018. Advances in optogenetic and chemogenetic methods to study brain circuits in non-human primates. J. Neural Transm. 125, 547–563.

Garrity, A.G., Pearlson, G.D., McKiernan, K., Lloyd, D., Kiehl, K.A., Calhoun, V.D., 2007. Aberrant “default mode” functional connectivity in schizophrenia. Am. J. Psychiatry 164, 450–457.

Giorgi, A., Migliarini, S., Galbusera, A., Maddaloni, G., Mereu, M., Margiani, G., Gritti, M., Landi, S., Trovato, F., Bertozzi, S.M., Armirotti, A., Ratto, G.M., De Luca, M.A., Tonini, R., Gozzi, A., Pasqualetti, M., 2017. Brain-wide Mapping of Endogenous Serotonergic Transmission via Chemogenetic fMRI. Cell Rep. 21, 910–918.

Gomez, J.L., Bonaventura, J., Lesniak, W., Mathews, W.B., Sysa-Shah, P., Rodriguez, L.A., Ellis, R.J., Richie, C.T., Harvey, B.K., Dannals, R.F., Pomper, M.G., Bonci, A., Michaelides, M., 2017. Chemogenetics revealed: DREADD occupancy and activation via converted clozapine. Science (80-.). 357, 503–507.

Gonzalez-Burgos, G., Cho, R.Y., Lewis, D.A., 2015. Alterations in cortical network oscillations and parvalbumin neurons in schizophrenia. Biol. Psychiatry 77, 1031–1040.

Gozzi, A., Schwarz, A.J., 2016. Large-scale functional connectivity networks in the rodent brain. Neuroimage 127, 496–509.

Gozzi, A., Schwarz, A.J., 2015. Large-scale functional connectivity networks in the rodent brain. Neuroimage.

Gradinaru, V., Thompson, K.R., Deisseroth, K., 2008. eNpHR: a Natronomonas halorhodopsin enhanced for optogenetic applications. Brain Cell Biol. 36, 129–139.

Grayson, D.S., Bliss-Moreau, E., Machado, C.J., Bennett, J., Shen, K., Grant, K.A., Fair, D.A., Amaral, D.G., 2016. The Rhesus Monkey Connectome Predicts Disrupted Functional Networks Resulting from Pharmacogenetic Inactivation of the Amygdala. Neuron 91, 453–466.

Gusnard, D.A., Raichle, M.E., 2001. Searching for a baseline: functional imaging and the resting human brain. Nat Rev Neurosci. 2(10):685-94.

Gutierrez-Barragan, D., Basson, M.A., Panzeri, S., Gozzi, A., 2019. Infraslow State Fluctuations Govern Spontaneous fMRI Network Dynamics. Curr. Biol. 29, 2295–2306.e5.

Hagmann, P., Cammoun, L., Gigandet, X., Meuli, R., Honey, C.J., Van Wedeen, J., Sporns, O., 2008. Mapping the structural core of human cerebral cortex. PLoS Biol. 6, 1479–1493.

Huang, X.-Q., Lui, S., Deng, W., Chan, R.C.K., Wu, Q.-Z., Jiang, L.-J., Zhang, J.-R., Jia, Z.-Y., Li, X.-L., Li, F., Chen, L., Li, T., Gong, Q.-Y., 2010. Localization of cerebral functional deficits in treatment-naive, first-episode schizophrenia using resting-state fMRI. Neuroimage 49, 2901–2906.

Hutchison, R.M., Mirsattari, S.M., Jones, C.K., Gati, J.S., Leung, L.S., 2010. Functional networks in the anesthetized rat brain revealed by independent component analysis of resting-state fMRI. J. Neurophysiol. 103, 3398–3406.

Just, M.A., Cherkassky, V.L., Keller, T.A., Kana, R.K., Minshew, N.J., 2006. Functional and Anatomical Cortical Underconnectivity in Autism: Evidence from an fMRI Study of an Executive Function Task and Corpus Callosum Morphometry. Cereb. Cortex 17, 951–961.

Leblond, C.S., Nava, C., Polge, A., Gauthier, J., Huguet, G., Lumbroso, S., Giuliano, F., Stordeur, C., Depienne, C., Mouzat, K., 2014. Meta-analysis of SHANK mutations in autism spectrum disorders: a gradient of severity in cognitive impairments. PLoS Genet. 10, e1004580.

Lee, J.H., 2012. Informing brain connectivity with optogenetic functional magnetic resonance imaging. Neuroimage 62, 2244–2249.

Lee, J.H., Durand, R., Gradinaru, V., Zhang, F., Goshen, I., Kim, D.S., Fenno, L.E., Ramakrishnan, C., Deisseroth, K., 2010. Global and local fMRI signals driven by

neurons defined optogenetically by type and wiring. Nature 465, 788–792.

Leichsenring, F., Leibing, E., Kruse, J., New, A.S., Leweke, F., 2011. Borderline personality disorder. Lancet 377, 74–84.

Liang, Z., Watson, G.D.R., Alloway, K.D., Lee, G., Neuberger, T., Zhang, N., 2015. Mapping the functional network of medial prefrontal cortex by combining optogenetics and fMRI in awake rats. Neuroimage 117, 114–123.

Lis, E., Greenfield, B., Henry, M., Guilé, J.M., Dougherty, G., 2007. Neuroimaging and genetics of borderline personality disorder: A review. J. Psychiatry Neurosci. 32, 162–173.

Liska, A., Bertero, A., Gomolka, R., Sabbioni, M., Galbusera, A., Barsotti, N., Panzeri, S., Scattoni, M.L., Pasqualetti, M., Gozzi, A., 2018. Homozygous Loss of Autism-Risk Gene CNTNAP2 Results in Reduced Local and Long-Range Prefrontal Functional Connectivity. Cereb. Cortex 28, 1141–1153.

Liska, A., Galbusera, A., Schwarz, A.J., Gozzi, A., 2015. Functional connectivity hubs of the mouse brain. Neuroimage 115, 281–291.

Liska, A., Gozzi, A., 2016. Can mouse imaging studies bring order to autism connectivity chaos? Front. Neurosci. 10, 484.

Lu, H., Zou, Q., Gu, H., Raichle, M.E., Stein, E.A., Yang, Y., 2012. Rat brains also have a default mode network. Proc. Natl. Acad. Sci. 109, 3979–3984.

Lynall, M.E., Bassett, D.S., Kerwin, R., McKenna, P.J., Kitzbichler, M., Muller, U., Bullmore, E., 2010. Functional Connectivity and Brain Networks in Schizophrenia. J. Neurosci. 30, 9477–9487.

Lynch, C.J., Uddin, L.Q., Supekar, K., Khouzam, A., Phillips, J., Menon, V., 2013. Default Mode Network in Childhood Autism: Posteromedial Cortex Heterogeneity and Relationship with Social Deficits. Biol. Psychiatry 74, 212–219.

Marenco, S., Stein, J.L., Savostyanova, A.A., Sambataro, F., Tan, H.Y., Goldman, A.L., Verchinski, B.A., Barnett, A.S., Dickinson, D., Apud, J.A., Callicott, J.H., Meyer-Lindenberg, A., Weinberger, D.R., 2011. Investigation of Anatomical Thalamo-Cortical Connectivity and fMRI Activation in Schizophrenia. Neuropsychopharmacology.

Nagel, G., Brauner, M., Liewald, J.F., Adeishvili, N., Bamberg, E., Gottschalk, A., 2005. Light Activation of Channelrhodopsin-2 in Excitable Cells of Caenorhabditis elegans Triggers Rapid Behavioral Responses. Curr. Biol. 15, 2279–2284.

Pagani, M., Bertero, A., Liska, A., Galbusera, A., Sabbioni, M., Barsotti, N., Colenbier, N., Marinazzo, D., Scattoni, M.L., Pasqualetti, M., Gozzi, A., 2019. Deletion of Autism Risk Gene Shank3 Disrupts Prefrontal Connectivity. J. Neurosci. 39 (27) 5299-5310

Peca, J., Feliciano, C., Ting, J.T., Wang, W., Wells, M.F., Venkatraman, T.N., Lascola, C.D., Fu, Z., Feng, G., 2011. Shank3 mutant mice display autistic-like behaviours and striatal dysfunction. Nature 472, 437–442.

Penagarikano, O., Lzaro, M.T., Lu, X.H., Gordon, A., Dong, H., Lam, H.A., Peles, E., Maidment, N.T., Murphy, N.P., Yang, X.W., Golshani, P., Geschwind, D.H., 2015. Exogenous and evoked oxytocin restores social behavior in the Cntnap2 mouse model of autism. Sci. Transl. Med. 7, 271ra8-271ra8.

Power, J.D., Schlaggar, B.L., Petersen, S.E., 2014. Studying brain organization via spontaneous fMRI signal. Neuron 84, 681–696.

Quiroga, R.Q., Nadasdy, Z., Ben-Shaul, Y., 2004. Unsupervised spike detection and sorting with wavelets and superparamagnetic clustering 271. Neural Comput. 16, 1661–1687.

Raichle, M.E., 2015. The brain’s default mode network. Annu Rev Neurosci 38, 433–447.

Raichle, M.E., MacLeod, A.M., Snyder, A.Z., Powers, W.J., Gusnard, D.A., Shulman, G.L., 2001. A default mode of brain function. Proc. Natl. Acad. Sci. U. S. A. 98, 676–82.

Rilling, J.K., Barks, S.K., Parr, L.A., Preuss, T.M., Faber, T.L., Pagnoni, G., Bremner, J.D., Votaw, J.R., 2007. A comparison of resting-state brain activity in humans and chimpanzees. Proc. Natl. Acad. Sci. U. S. A. 104, 17146–17151.

Rodenas-Cuadrado, P., Ho, J., Vernes, S.C., 2014. Shining a light on CNTNAP2: complex functions to complex disorders. Eur. J. Hum. Genet. 22, 171–178.

Roth, B.L., Craigo, S.C., Choudhary, M.S., Uluer, A., Monsma, F.J., Shen, Y., Meltzer, H.Y., Sibley, D.R., 1994. Binding of typical and atypical antipsychotic agents to 5-hydroxytryptamine-6 and 5-hydroxytryptamine-7 receptors. J. Pharmacol. Exp. Ther. 268, 1403–1410.

Schleifer, C., Lin, X.A., Kushan, L., Ji, X.J.L., Yang, G., Bearden, X.C.E., 2019. Dissociable Disruptions in Thalamic and Hippocampal Resting-State Functional Connectivity in Youth with 22q11 . 2 Deletions 39, 1301–1319.

Schwarz, A.J., Gass, N., Sartorius, A., Risterucci, C., Spedding, M., Schenker, E., Meyer-Lindenberg, A., Weber-Fahr, W., 2013. Anti-correlated cortical networks of intrinsic connectivity in the rat brain. Brain Connect. 3, 503–511.

Schwarz, A.J., Gozzi, A., Chessa, A., Bifone, A., 2012. Voxel Scale Complex Networks of Functional Connectivity in the Rat Brain: Neurochemical State Dependence of Global and Local Topological Properties. Comput. Math. Methods Med. 2012.

Scott-Van Zeeland, A.A., Abrahams, B.S., Alvarez-Retuerto, A.I., Sonnenblick, L.I., Rudie, J.D., Ghahremani, D., Mumford, J.A., Poldrack, R.A., Dapretto, M., Geschwind, D.H., Bookheimer, S.Y., 2010. Altered Functional Connectivity in Frontal Lobe Circuits Is Associated with Variation in the Autism Risk Gene CNTNAP2. Sci. Transl. Med. 2, 56ra80-56ra80.

Sforazzini, F., Bertero, A., Dodero, L., David, G., Galbusera, A., Scattoni, M., Pasqualetti, M., Gozzi, A., 2014a. Altered functional connectivity networks in acallosal and socially impaired BTBR mice. Brain Structure & Function 1–14.

Sforazzini, F., Schwarz, A.J., Galbusera, A., Bifone, A., Gozzi, A., 2014b. Distributed BOLD and CBV-weighted resting-state networks in the mouse brain. Neuroimage 87, 403–415.

Shehzad, Z., Kelly, A.M.C., Reiss, P.T., Gee, D.G., Gotimer, K., Uddin, L.Q., Lee, S.H., Margulies, D.S., Roy, A.K., Biswal, B.B., Petkova, E., Castellanos, F.X., Milham, M.P., 2009. The resting brain: Unconstrained yet reliable. Cereb. Cortex 19, 2209–2229.

Stafford, J.M., Jarrett, B.R., Miranda-Dominguez, O., Mills, B.D., Cain, N., Mihalas, S., Lahvis, G.P., Lattal, K.M., Mitchell, S.H., David, S. V, Fryer, J.D., Nigg, J.T., Fair, D.A., 2014. Large-scale topology and the default mode network in the mouse connectome. Proc. Natl. Acad. Sci. 111, 18745–18750.

Sternson, S.M., Roth, B.L., 2014. Chemogenetic tools to interrogate brain functions. Annu. Rev. Neurosci. 37, 387–407.

Strauss, K.A., Puffenberger, E.G., Huentelman, M.J., Gottlieb, S., Dobrin, S.E., Parod, J.M., Stephan, D.A., Morton, D.H., 2006. Recessive symptomatic focal epilepsy and mutant contactin-associated protein-like 2. N. Engl. J. Med. 354, 1370–1377.

Tabet, A.-C., Rolland, T., Ducloy, M., Lévy, J., Buratti, J., Mathieu, A., Haye, D., Perrin, L., Dupont, C., Passemard, S., 2017. A framework to identify contributing genes in patients with Phelan-McDermid syndrome. NPJ genomic Med. 2, 32.

Tomasi, D., Volkow, N.D., 2011. Functional connectivity hubs in the human brain. Neuroimage 57, 908–917.

Toro, R., Konyukh, M., Delorme, R., Leblond, C., Chaste, P., Fauchereau, F., Coleman, M., Leboyer, M., Gillberg, C., Bourgeron, T., 2010. Key role for gene

dosage and synaptic homeostasis in autism spectrum disorders. Trends Genet. 26, 363–372.

Uddin, L.Q., Kelly, A.M., Biswal, B.B., Castellanos, F.X., Milham, M.P., 2009. Functional connectivity of default mode network components: correlation, anticorrelation, and causality. Hum. Brain Mapp. 30, 625–637.

van den Heuvel, M.P., Hulshoff Pol, H.E., 2010. Exploring the brain network: A review on resting-state fMRI functional connectivity. Eur. Neuropsychopharmacol. 20, 519–534.

van den Heuvel, M.P., Sporns, O., 2013. Network hubs in the human brain. Trends Cogn. Sci. 17, 683–696.

Vardy, E., Robinson, J.E., Li, C., Olsen, R.H.J., DiBerto, J.F., Giguere, P.M., Sassano, F.M., Huang, X.-P., Zhu, H., Urban, D.J., White, K.L., Rittiner, J.E., Crowley, N.A., Pleil, K.E., Mazzone, C.M., Mosier, P.D., Song, J., Kash, T.L., Malanga, C.J., Krashes, M.J., Roth, B.L., 2015. A New DREADD Facilitates the Multiplexed Chemogenetic Interrogation of Behavior. Neuron 86, 936–946.

Vincent, J.L., Patel, G.H., Fox, M.D., Snyder, A.Z., Baker, J.T., Van Essen, D.C., Zempel, J.M., Snyder, L.H., Corbetta, M., Raichle, M.E., 2007. Intrinsic functional architecture in the anaesthetized monkey brain. Nature 447, 83–86.

Wang, L., Hermens, D.F., Hickie, I.B., Lagopoulos, J., 2012. A systematic review of resting-state functional-MRI studies in major depression. J. Affect. Disord. 142, 6–12.

Welsh, R.C., Chen, A.C., Taylor, S.F., 2008. Low-Frequency BOLD Fluctuations Demonstrate Altered Thalamocortical Connectivity in Schizophrenia. Schizophr. Bull. 36, 713–722.

Yeo, B.T.T., Krienen, F.M., Sepulcre, J., Sabuncu, M.R., Lashkari, D., Hollinshead, M., Roffman, J.L., Smoller, J.W., Zollei, L., Polimeni, J.R., Fischl, B., Liu, H., Buckner, R.L., 2011. The organization of the human cerebral cortex estimated

by intrinsic functional connectivity. J. Neurophysiol. 106, 1125–1165.

Yizhar, O., Fenno, L.E., Davidson, T.J., Mogri, M., Deisseroth, K., 2011a. Optogenetics in neural systems. Neuron 71, 9–34.

Yizhar, O., Fenno, L.E., Prigge, M., Schneider, F., Davidson, T.J., 'Shea, D.J., Sohal, V.S., Goshen, I., Finkelstein, J., Paz, J.T., Stehfest, K., Fudim, R., Ramakrishnan, C., Huguenard, J.R., Hegemann, P., Deisseroth, K., 2011b. Neocortical excitation/inhibition balance in information processing and social dysfunction. Nature 477, 171–178.

Zerbi, V., Floriou-Servou, A., Markicevic, M., Vermeiren, Y., Sturman, O., Privitera, M., von Ziegler, L., Ferrari, K.D., Weber, B., De Deyn, P.P., Wenderoth, N., Bohacek, J., 2019. Rapid Reconfiguration of the Functional Connectome after Chemogenetic Locus Coeruleus Activation. Neuron 103, 702–718.e5.

Zhao, W., Luo, L., Li, Q., Kendrick, K., 2013. What Can Psychiatric Disorders Tell Us about Neural Processing of the Self? . Front. Hum. Neurosci. .

Zikopoulos, B., Barbas, H., 2013. Altered neural connectivity in excitatory and inhibitory cortical circuits in autism. Front. Hum. Neurosci. 7.